Journal of Materials Research and Technology 27 (2023) 7138–7158

Contents lists available at ScienceDirect

Journal of Materials Research and Technology

journal homepage: www.elsevier.com/locate/jmrt

An analysis of microstructural morphology, surface topography, surface integrity, recast layer, and machining performance of graphene nanosheets on Inconel 718 superalloy: Investigating the impact on EDM characteristics, surface characterizations, and optimization

Kamlesh Paswan [a,**,1], Shubham Sharma [b,c,d,*,1], Shashi Prakash Dwivedi [e], Maha Khalid Abdulameer [f], Changhe Li [c], Yaser Yasin [g], Mohamed Abbas [h,***], Elsayed M. Tag-Eldin [i,****]

[a] Sandip Institute of Engineering and Management, Nashik, 422213, India
[b] Dept. of Mechanical Eng., University Centre for Research and Development (UCRD), Chandigarh University, Mohali, India
[c] School of Mechanical and Automotive Engineering, Qingdao University of Technology, Qingdao, 266520, China
[d] Department of Mechanical Engineering, Lebanese American University, Kraytem, 1102-2801, Beirut, Lebanon
[e] Lloyd Institute of Engineering & Technology, Knowledge Park II, Greater Noida, Uttar Pradesh 201306, India
[f] Al-Noor University College, Nineveh, Iraq
[g] Al-Farahidi University, Iraq
[h] Electrical Engineering Department, College of Engineering, King Khalid University, Abha City, 61421, Saudi Arabia
[i] Faculty of Engineering, Future University in Egypt, New Cairo, 11835, Egypt

ARTICLE INFO

Handling Editor: SN Monteiro

Keywords:
Electrical discharge machining
Powder mixed EDM
Machining
Graphene
Nanofluid
Material removal rate

ABSTRACT

Inconel 718 finds extensive applications in the aviation and aerospace industries, particularly in the manufacturing of jet engines and high-speed airframe components like fasteners, bolts, buckets, instrumentation parts, wheels, and spacers. It is also utilised in the production of cryogenic tankage and gas turbine blades. The present study focuses on investigating the machining performance of graphene nanosheets on Inconel 718. Various aspects of Inconel 718's machinability through electrical discharge machining (EDM) have been examined, including material removal rate (MRR), surface roughness, surface morphology, tool rear Rate (TWR), residual stresses on the machined surface, Vickers hardness, and recast layer thickness. The investigation reveals a significant impact of process parameters on these machining characteristics. The effects of graphene nanosheets have been observed using several analytical instruments such as field emission scanning electron microscopy (FE-SEM), transmission electron microscopy (TEM), particle size analyzer, and X-ray diffraction (XRD). Furthermore, optimization of the response data with respect to input parameters has been performed in this study. TEM analysis is used to determine the size of individual debris particles in deionised water and mixed graphene nanosheet dielectric mediums. To verify that the debris particles are the same as the parent material, energy dispersive X-ray spectroscopy (EDX) is used. To determine the compounds and crystal structures present in the base metal and machined surfaces, XRD analysis is used. A high-resolution X-ray diffractometer (HRXRD) is used to measure the residual stresses on the machined surface. EDX composition testing is used to analyze surface modification. Due to the rapid heating and quenching that takes place in the dielectric medium, the machined surface becomes harder. Deposited materials, microholes, and surface textures can all be observed through FESEM microstructure observation. Comparing conventional EDM to nanosheets mixed dielectric, the thickness

* Corresponding authors. Dept. of Mechanical Eng., University Centre for Research and Development (UCRD), Chandigarh University, Mohali, India.
** Corresponding author.
*** Corresponding authors.
**** Corresponding author.
E-mail addresses: kamleshpgcr@gmail.com (K. Paswan), shubham543sharma@gmail.com, shubhamsharmacsirclri@gmail.com (S. Sharma), spdglb@gmail.com (S.P. Dwivedi), maha.khalid@alnoor.edu.iq (M.K. Abdulameer), sy_lichanghe@163.com (C. Li), zahraabdulradih@gmail.com (Y. Yasin), mabas@kku.edu.sa (M. Abbas), elsayed.tageldin@fue.edu.eg (E.M. Tag-Eldin).
[1] Equally contributed.

https://doi.org/10.1016/j.jmrt.2023.11.080
Received 12 August 2023; Received in revised form 2 November 2023; Accepted 9 November 2023
Available online 14 November 2023

of the recast layer is reduced. To recapitulate, the study explores how various machining parameters and dielectric mediums affect EDM processes. It examines debris particle size, compound formation, residual stresses, surface modification, hardness, microstructure, and recast layer thickness. The addition of graphene nanosheets to the dielectric medium produces promising results, reducing the thickness of the recast layer and improving surface quality. The results offer suggestions for improving Inconel 718 material surface properties and EDM machining effectiveness.

1. Introduction

Electrical discharge machining (EDM) is a thermo-electrical erosion process renowned for its remarkable ability to effectively machine highly resistant conductive materials like Inconel alloy, Ti alloy, and other superalloys, regardless of their hardness. This technique has proven to be a valuable alternative to conventional methods such as drilling, milling, and polishing. One of its key advantages lies in the absence of direct contact between the tool and workpiece, enabling the precision machining of delicate materials. Moreover, EDM minimizes residual stress and mitigates the impact of vibrations. The introduction of impurities into the dielectric medium in powder mixed EDM (PMEDM) has further amplified machining performance [1]. The presence of suspended particles in the dielectric medium significantly reduces breakdown strength, leading to the occurrence of multiple discharges. This division of a single discharge into multiple discharges effectively decreases the thermal energy per discharge, resulting in the formation of shallow craters during the PMEDM process [2]. The machining performance also get affected the by workpiece material's properties. The low thermal conductivity of super alloys like Inconel 718 is a significant hindrance when using the EDM process [1,2]. Inconel 718 is a high-strength, Ni-based superalloy that is known for its exceptional resistance to extreme temperatures, corrosion, and mechanical stress. However, its low thermal conductivity presents challenges during EDM operations. Inconel 718's low thermal conductivity means that it does not conduct heat away from the EDM site as efficiently as materials with higher thermal conductivity [1,2]. As a result, the intense heat generated during EDM tends to accumulate in the material, leading to localised overheating [2,3].

In addition, Inconel 718 is a commonly employed Ni-based superalloy notable for its remarkable mechanical capabilities at higher temperatures and its resistance to corrosion [1]. Nevertheless, one noticeable attribute of this material includes its relatively poor thermal conductivity, which poses difficulties with the implementation of EDM technique.

i. Low Thermal Conductivity and EDM Efficiency:

The thermal conductivity of Inconel 718 is comparatively lower in relation to other materials typically undergoing EDM, such as Al, Cu, and certain steel alloys [1]. The material's thermal conductivity is estimated to be around 6 W/m.K, which is much lower when compared to highly conductive materials such as Cu (398 W/m.K) [1]. The reduced thermal conductivity has a detrimental impact on the effectiveness of EDM processes. At room temperature (RT), the thermal conductivity of Inconel 718 is around 6.7 W/m.K, which is notably lower compared to the thermal conductivity of standard tool steels often employed in EDM procedure [1,2]. The primary source of this characteristic may be attributed to its higher concentrations of Ni and Cr, leading to a comparatively lowered phonon mean free path [1,2].

The operation of EDM is predicated upon the generation of electrical sparks that occur among the tool electrode and the workpiece. The formation of such sparks conduces to the production of high levels of thermal energy, causing the material from the workpiece to undergo the processes of melting and vaporization [1,2]. The stabilisation of the method is contingent upon the efficient dissipation of heat. The limited thermal conductivity of Inconel 718 restricts its capacity to efficiently disperse heat, resulting in localised overheating [1,2]. The alloy's limited thermal conductivity hampers its capacity to effectively disperse the heat produced during the EDM process [1,2]. As a result, the temperature in the specific area where machining occurs has a tendency to rise quickly, culminating in various negative consequences [1,2].

ii. The process of recasting layer formation:

The application of EDM on Inconel 718 has been observed to lead to the development of a recast layer on the surface that has been machined. The behaviour in concern is attributed to the limited thermal conductivity, which imposes restrictions on the efficient dissipation of heat [1–3]. The use of EDM on Inconel 718 has been perceived as resulting in the formation of a recast layer on the machined surface. The presence of a restricted thermal conductivity further accentuates the development in this layer, which is composed of molten material that has hardened again and may possess unfavourable characteristics [1–3].

During the method of EDM, a phenomenon occurs where a portion of the removed material undergoes re-solidification on the surface being machined, resulting in the formation of a recast layer [1–3]. The poor thermal conductivity demonstrated by Inconel 718 hampers the rate of cooling, hence facilitating the development of a particular layer. This layer has the potential to impact both the surface finish and the structural integrity of the material [1–3]. The prolonged duration of material's exposure to the EDM process is attributed to the slower dissipation of heat, thereby raising the probability of recast layer production. The mechanical and metallurgical characteristics of this layer may be modified, potentially rendering them inappropriate for the intended applications [1–3].

iii. The phenomenon of electrode wear and tool life.

The diminished thermal conductivity demonstrated by Inconel 718 conduces to heightened tool wear and a shorter operational lifespan of EDM electrodes [1–3]. The phenomenon of electrode wear is expedited by prolonged exposure to higher temperatures, as confirmed by scientific evidence. The insufficient thermal conductivity of Inconel 718 contributes to the concentration of heat within a limited restricted area during the EDM process, hence causing an accelerated deterioration of the tool electrode and a reduced lifespan of the tool or shortened tool life [4].

iv. Premature Tool Wear:

In the field of EDM, the process involves the generation of a plasma channel at higher temperatures by the application of an electrical discharge among the tool electrode and the workpiece [1–3]. In materials characterised by restricted thermal conductivity, such as Inconel 718, the plasma channel has the potential to reach extremely higher temperatures, leading to accelerated wearing of the tool electrode [1–3]. A rise in temperature expedites the erosion process of the tool electrode owing to the thermal softening of the electrode material, leading to an accelerated rate of wear [4]. As a consequence, there is a high frequency of tool changes, which causes escalated machining expenditures and lowered productivity [4].

v. The increased susceptibility to cracking:

The localised accumulation of thermal energy throughout the machining zone, caused by its relatively limited thermal conductivity, can lead to the development of thermal stresses and a higher susceptibility to cracking within the material of the workpiece [1–3]. The occurrence of thermal stresses in Inconel 718 as a consequence of rapid and uneven heating and cooling cycles has the potential to induce micro-cracks or macroscopic fracturing or rupturing or cracking, especially in components that are complicated or intricated, and thin-walled [1–3]. In summary, the limited heat conductivity exhibited by Inconel 718 poses a notable impediment to its efficient utilisation in EDM method [2–4].

In the last decade, there have been notable breakthroughs in the field of EDM technology. The primary aim of these advancements has been to enhance the efficiency, productivity, precision, and surface polish of machining processes, while simultaneously addressing environmental considerations and cost-effectiveness [3]. One significant development is the incorporation of advanced control algorithms and adaptive techniques, including adaptive pulse generation and adaptive tool-path planning [3]. The aforementioned developments in technology have played a significant role in reducing the duration required for machining operations and strengthening the overall stability of the manufacturing process. In addition, the inclusion of real-time monitoring and feedback systems has facilitated the development of precisely control over the discharge process, which has resulted in enhanced levels of precision and surface quality [1,2].

Recent studies have demonstrated the application of "Artificial Intelligence", (AI) and "Machine Learning" (ML) algorithms within the domain of EDM [4,5]. These studies have successfully utilised these algorithms to predict the most favourable machining settings by employing real-time sensor data. This approach not only enhances the optimization of the process, however it also mitigates the wear of tools and electrodes, so enhancing both the efficiency and longevity of the tools [5–7].

The superalloy named, Inconel 718 offers significant challenges owing to its exceptional high-temperature characteristics, remarkable heat-resistance, and notable toughness [5–7]. The utilisation of EDM has demonstrated its efficacy as a machining technique for this particular superalloy, however, without encountering certain roadblocks. The scientific discourse and underlying mechanisms pertaining to the performance of EDM on Inconel 718 may be elucidated as follows:

i. **Thermal Energy Generation:** Thermal energy generation occurs in the context of EDM, where the interaction among the electrode and workpiece results in the generation of significant levels of heat [5–7]. The application of concentrated heat causes the material to undergo a phase transition, wherein it transitions from a solid state to a liquid and subsequently to a gaseous state, resulting in the development of a depression hollow-opening, grooves, cavities, crevices, craters, and recessions on the surface [8]. The relatively high melting point of Inconel 718 necessitates the utilisation of higher-energy discharges, which might result in the occurrence of thermal-stresses and the formation of recast layers [8,9].
ii. **Dielectric Fluid Influence:** The impact of dielectric fluid is of paramount significance in the context of EDM. It functions as a coolant and effectively removes debris [10]. The selection of dielectric and its associated factors, including dielectric strength and flushing rate, have an enormous influence on the performance of the machining process [10]. In a recent study, the investigation focused on the utilisation of modern dielectric fluids possessing enhanced thermal characteristics. The objective was to address the challenges associated with heat-related concerns encountered during the EDM process of Inconel 718 [11,12].
iii. **Tool Electrode Wear:** The abrasion characteristics of Inconel 718 may culminate in accelerated wear of the tool electrode [11,12]. Academic researchers are now engaged in the investigation of innovative electrode materials, including "polycrystalline diamond" (PCD), and "cubic boron nitride" (CBN), having the intent to enhance the wear resistance of electrodes and enhancing machining efficiency in the context of superalloy applications [12].

In addition, in the last decade, the field of EDM has experienced notable progressions. A significant advancement is the utilisation of advanced pulse generators and control algorithms, which provide enhanced precision for controlling the discharge procedure [11,12]. The application of adaptive control techniques, specifically model predictive control (MPC), has been growing in popularity throughout recent times [13]. The proposed methodology seeks to enhance the precision & surface-finish of machining operations by dynamically adjusting parameters associated with the parameters in response to sensor data in real-time [13].

Furthermore, the utilisation of innovative electrode materials and surface modifications has resulted in enhanced efficiency of EDM. An instance of this may be observed in the utilisation of Cu electrodes reinforced with Gr, which exhibit enhanced resistance to wear and greater thermal conductivity [13,14]. As a result, the lifespan durability of tools extends and machining efficiency is raised [13,14].

The evolution of EDM necessitates recognition of the ongoing potential for enhancements. An area that necessitates consideration is the environmental ramifications of EDM, specifically pertaining to the proper disposal of dielectric fluids and the management of electrode wear debris [11,12]. The advancement of EDM may be accomplished through the use of sustainable machining practises, including the utilisation of biodegradable dielectric fluids with the reuse and recycling of electrode materials [15].

In addition, continuing research is being done to optimise the machining settings specifically for materials such as Inconel 718. Recent research has investigated the impact of pulse length, discharge energy, and tool electrode wear on the EDM performance of the aforementioned superalloy [15]. The intent of this investigation is to optimise the operating variables or factors in order to enhance operational effectiveness and minimise tool degradation [15].

Machining Inconel 718 presents difficulties owing to its high thermal characteristics and exceptional corrosion resistance [16]. The process of EDM on Inconel 718 can frequently involve intricate interacts among the electrode, workpiece, and dielectric medium [17,18]. In order to enhance the efficiency of machining processes, current research endeavours have been directed towards:

i. **Pulse Power Modulation:** The method of pulse power modulation has been employed by researchers to enhance the material removal rates throughout machining, while simultaneously ensuring the maintenance of dimensional accurateness [11,12]. The utilisation of this method serves to mitigate the potential for thermal degradation to the material being worked with [17].
ii. **Tool Electrode Composition:** The investigation of enhanced electrode materials, including W-based alloys and diamond-like carbon coatings, has demonstrated potential in mitigating electrode wear and enhancing surface smoothness [18,19].
iii. **Adaptive Control:** The optimization of machining performance on Inconel 718 has been discovered by utilizing adaptive control techniques, which involve real-time continuous monitoring and management of EDM parameters. This is achieved by utilizing data from sensors and process models [11,12].

PMEDM significantly expands the capabilities of traditional EDM, yielding surfaces with nearly mirror-like finishes, thin recast layer thickness, high material removal rate (MRR), low tool wear rate (TWR), and improved interelectrode gap (IEG). Researchers have conducted extensive investigations into PMEDM, utilizing a wide array of powders,

such as SiC, Al_2O_3, carbon nanotubes (CNT), ZnO, TiO, Ag, SiO, and Gr. These powders are combined with various dielectric fluids, including kerosene, distilled water, deionised water, deionised water with glycerin, and water-oil mist, to further optimise the machining process [3].

The powder particles distributed the discharge over the workpiece, which widened the discharge gap. It also increases electric field intensity three times higher than conventional EDM [4]. Researchers have used many conductive powder in EDM such as Al [5,6], Gr [7–9], Si [10,11], Cu [12], SiC [13,14], Cr [15], B_4C [16], and W [17,18] also varied the powder composition with the base dielectric as shown in Table 1.

Response parameters such as higher MRR and lower surface roughness was achieved in comparison to the conventional EDM. The non-conductive powders Al_2O_3 and SiO [19,48] has been used in EDM process.

In recently, the application of nanofluid has increased drastically. Kumar and Batra [17] used W nanopowder of size range from 30 to 40 μm mixed in hydrocarbon oil to machine OHNS, D2 die steel and H13 material through EDM. The authors stated that the process can be used for surface modification [49,50], as the observation shows significant amount of W over machines surface. W percentage increases from negligible amount to 3.25 %. The authors also revealed the favourable condition for surface modification in EDM process such as short pulse on time, low discharge, negative polarity and longer pulse off time [51]. Peak current has significant effect of roughness. Prabhu et al. [52] mixed single-wall carbon nanotubes (CNTs) of length 5–30 μm, and diameter 1–2 nm into the kerosene dielectric medium machined Inconel 825 material through EDM process. The CNT present in the dielectric medium absorbs heat from electrically discharged material, resulting in a thin recast layer formation over the machined surface. It improves surface roughness from 0.48 to 0.12 μm, microcrack size from 294 to 79.2 nm and depth of microcracks from 1.2 to 330 nm. It was also stated that surface finish could be improved more at low pulse energy condition. Mai et al. [53] investigated CNT (length 1–3 μm and diameter 40–60 nm) nano powder's effect with kerosene dielectric medium to machine NAK80 steel. It improves machining efficiency by 66 % and surface roughness by 70 %. The smoother surface obtained at 0.2 and 0.4 g/L concentration of CNT nanopowder. Sari et al. [2] used multi-wall carbon nanotubes for their investigation. This investigation found that multi-wall CNTs (MWCNTs) give favourable MRR than conventional EDM due to the better electricity flow. It also has a better surface finish as the MWCNTs nanofluid effectively absorbs heat. Marashi et al. [54] and Jin et al. [55] machined D2 steel using Ti nanopowder mixed dielectric medium. The NPMEDM process improves the surface morphology such as microcracks, microholes and droplets over the machined surface. It also improves MRR and surface roughness by 69 and 35 %, respectively. The absence of the materials transfers from the tool to the machined surface was confirmed by XRD analysis. Marashi et al. [54] and Jin et al. [55] machined D2 steel using Ti nanopowder mixed dielectric medium. The NPMEDM process improves the surface morphology such as microcracks, microholes and droplets over the machined surface. It also improves MRR and surface roughness by 69 and 35 %, respectively. The absence of the materials transfers from the tool to the machined surface is confirmed by XRD analysis. Baseri and Sadeghian [46] studied the effect of a rotary tool and magnetic field in NPMEDM. The best result was obtained during the EDM process when the tool was rotated at 200 rpm in 1 g/l concentration of TiO_2 nanopowder mixed with kerosene dielectric medium at 0.38T magnetic field. MRR increases with the increase in rpm up to 200 rpm due to centrifugal force, removing debris from the machined zone. A further increase in rpm leads to bubble formation, affecting the plasma formation; therefore, MRR decreases. Mohal and Kumar [56] investigated CNT nano powder's effect on AL/10%SiC_p MMC workpiece. The CNT nanopowder improves machining performance by 38.22 %. Also, less than 1 μm surface roughness (0.411 μm) was achieved at 0.4 g/l concentration of CNT nanopowder into EDM oil. The overall roughness was improved by 46.06 % in NPMEDM compared with conventional EDM.

As indicated by existing literature, nanofluids have emerged as a superior alternative to conventional fluids. The base dielectric medium influences their performance. These fluids find extensive applications in both traditional and non-traditional machining processes. The improved thermal conductivity of nanofluids is attributed to the increased specific surface area of the powder particles. Additionally, reducing particle size contributes to achieving a better surface finish. Incorporating conductive nanoparticles further enhances the electrical conductivity of nanofluids, ultimately boosting the performance of EDM. Therefore, analysing the utilisation of nano-sized conductive particles with a high specific surface area is crucial. This study employs a multilayer graphene nanofluid (55–60 nm), using deionised water as the base medium. The experimental design follows the Box-Behnken methodology, a type of response surface methodology (RSM). The MRR and surface texture are key evaluation parameters for assessing the impact of major process control factors.

2. Experimentation: materials and methods

Graphene, a carbon allotrope, possesses a unique two-dimensional honeycomb structure with exceptional chemical and mechanical characteristics, including high electrical and thermal conductivity (5000W/(m.K)). The process of synthesizing graphene nanofluid involves blending graphene nanopowder into deionised water as the base fluid, with ultrasonication employed to establish and maintain dispersion. Nanoparticles exhibit various shapes, and of these, sphericity has the smallest surface area. To mitigate this, a grinding method is employed to transform sphericity and other shapes into flat particles, thereby increasing the surface area and, consequently, enhancing the thermal dissipation properties of the nanofluid. It's worth noting that graphene differs slightly from CNTs in terms of surface area, with graphene particles boasting nearly double the surface area compared to single-walled CNTs. For experimentation, samples are prepared, including one sample of pure deionised water and four samples of Graphene nanofluid (50–60 nm) mixed at varying volumes (10, 20, 30, and 40 ml) with 800 ml of deionised water. The experiments are conducted using an SPARKONIX ZNC/ENC35 Sink EDM machine, with a custom-made tank measuring $20 \times 20 \times 10$ cm^3 constructed from Perspex sheet material. To remove debris from the machined area, an 18W completely submersible pump is employed. The workpiece chosen for machining is composed of Inconel 718 material, while the tool measures 12×5 mm^2 and is made of Cu.

The input parameters were chosen based on the literature review. Lower peak currents (2A–6A), lower pulse on time (4μ to 12μs) and gap

Table 1
Base dielectric used for PMEDM.

1. Mixture of air and mineral Oil (5 %)	2.Deionised Water (12 %)	3. Hydrocarbon Based Oil (86 %)	
Si + Air + water [20], Si + deionised water + air [21]	SiC [22], B_4C [16,23], Ti [24], Si [25]	**3(a) Mineral oil** Gr, Si, Al, SiC, MoS_2, crushed glass [26], Ti [27], Al, Cu, Cr, SiC [5], Gr [28,29], Si [14], Gr nanofiber [8,30], Al [31], Gr, Al [32,33]	**3(b)Kerosene** Gr [34,35], Al, SiC [6], Al [36], Al, Cu, Cr, SiC [37], Si [11,12,38,39] TiC [40], MoS_2 [41], B_4C [16,23], Cr [17,42], Al [43], Si [44], Gr [45], TiO_2 [46], Al_2O_3 [47]

Table 2
Input parameters.

Parameters	Level 1	Level 2	Level 3
T_{on} (μs)	4	8	12
I_p (A)	2	4	6
Gv (V)	10	30	50

voltage (10V–50V) were selected. Table 2 shows the input parameters and their levels. Machining is performed at a concentration of 0.2 g per 800 ml deionised water.

3. Results and discussions

In order to identify the influential process parameters in graphene Nano-Scale Material Electrical Discharge Machining (NSMEDM), a comprehensive analysis has been conducted, encompassing both qualitative and quantitative aspects. RSM (Response Surface Methodology) models have been established and employed to assess crucial factors such as MRR, TWR, and surface roughness. Additionally, the machined surface morphology is examined using FESEM and ImageJ software for further analysis.

The experimental design presented in Table 3 is based on the Box-Behnken method, utilizing RSM. To evaluate the effectiveness of graphene nanosheets, the output data from deionised water experiments are compared with those from graphene nanosheets in Tables 4 and 5. The results demonstrate notable improvements in various parameters. The MRR shows enhancements ranging from 2.62 to 114.29 %, while surface roughness parameters, such as Ra, Rq, and Rz, exhibit enhancements ranging from 0.99 to 31.47 %, 0.93–35.88 %, and −0.21 to 31.47 %, respectively. These improvements can be attributed to the enhanced thermal and electrical conductivity of graphene nanosheets. During the machining process, the nanosheets act as conductors between the tool and the workpiece, facilitating more efficient current transfer with minimal resistance compared to deionised water alone. As a result, the MRR is significantly increased. Table 3 exhibits the response values for MRR and Surface roughness (Ra, Rq and Rz).

The regression equation for MRR and surface roughness is determined from Table 3. These regression equations further process the relationship between input and output parameters plotted in a graph. The regression equations are developed to predict the response parameters. Additionally, the expected value tested and found lies between 95 % of CI at 8μ, 6A and 10V. The error for the responses is less than ±5 %. The CI and PI show the relative adequacy between the actual and predicted values.

Regression equations for MRR, Ra, Rq and Rz for the dielectric without nanosheets in Uncoded units

$$\text{MRR DI water} = -21.17 + 1.083\ A + 5.10\ B + 0.669C - 0.0013\ A \times A - 0.411\ B \times B - 0.00307C \times C + 0.4167\ A \times B - 0.04375\ A \times C - 0.0656\ B \times C \quad (1)$$

$$\text{Ra DI water} = 2.38 + 0.235\ A + 0.004\ B - 0.0311C - 0.01199\ A \times A - 0.0068\ B \times B - 0.000149C \times C - 0.0160\ A \times B + 0.00101\ A \times C + 0.00345\ B \times C \quad (2)$$

Table 4
MRR and Ra measured on the specimens without graphene and with graphene.

MRR DI water (mg/min) (A)	MRR Graphene (mg/min) (B)	Improvement [(B-A)/A] *100	Ra DI water (μm) (A)	Ra Graphene (μm) (B)	Improvement [(A-B)/B] *100
6.50	8.20	26.15	2.67	2.19	17.98
6.50	6.67	**2.62**	1.81	1.60	11.60
12.00	18.33	52.75	2.86	1.96	**31.47**
9.50	12.50	31.58	2.11	2.04	3.32
11.00	13.33	21.18	1.94	1.92	1.03
3.00	4.17	39.00	2.24	1.91	14.73
3.50	5.12	46.29	3.01	2.87	4.65
27.33	34.50	26.23	2.03	2.01	**0.99**
12.50	13.33	6.64	2.05	1.91	6.83
5.50	7.37	34.00	1.99	1.61	19.10
14.50	20.86	43.86	2.16	1.91	11.57
21.00	45.00	**114.29**	2.52	2.43	3.57
7.50	9.17	22.27	2.67	2.55	4.49
25.00	32.50	30.00	2.49	2.36	5.22
14.00	19.56	39.71	2.42	2.06	14.88

Table 5
Rq and Rz measured on the specimens without graphene and with graphene.

Rq DI water (μm) (A)	Rq Graphene (μm) (B)	Improvement [(A-B)/B] × 100	Rz DI water (μm) (A)	Rz Graphene (μm) (B)	Improvement [(AB)/B] × 100
3.25	2.69	17.23	15.35	13.66	11.01
2.27	2.03	10.57	10.90	9.02	17.25
3.54	2.27	**35.88**	15.80	11.47	27.41
2.58	2.47	4.26	17.99	11.17	**37.91**
2.45	2.35	4.08	11.64	10.43	10.40
2.79	2.36	15.41	12.09	10.99	9.10
3.69	3.56	3.52	17.52	16.55	5.54
2.63	2.58	1.90	12.39	12.09	2.42
2.56	2.38	7.03	11.91	11.63	2.35
2.55	2.01	21.18	13.42	9.61	28.39
2.35	2.24	4.68	11.67	9.98	14.48
3.11	3.08	0.96	14.99	14.32	4.47
3.22	3.19	**0.93**	13.98	14.01	**−0.21**
3.04	3.02	0.66	14.11	13.68	3.05
2.97	2.17	26.94	14.60	11.66	20.14

$$\text{Rq DI water} = 3.49 + 0.216\ A - 0.172\ B - 0.0422C - 0.0119\ A \times A + 0.0091\ B \times B - 0.000042C \times C - 0.0121\ A \times B + 0.00121\ A \times C + 0.00365\ B \times C \quad (3)$$

And

Table 3
MRR and surface roughness measured on the specimens without graphene and with graphene.

Input parameters			Response values for deionised water				Response values for deionised water with 0.2 g graphene			
T_{on} (μs)	I_p (A)	Gv (V)	Ra DI water (μm)	Rq DI water (μm)	Rz DI water (μm)	MRR DI water (mg/min)	Ra Graphene (μm)	Rq Graphene (μm)	Rz Graphene (μm)	MRR Graphene (mg/min)
4	4	10	2.67	3.25	15.35	6.50	2.19	2.69	13.66	8.20
4	4	50	1.81	2.27	10.90	6.50	1.60	2.03	9.02	6.67
8	4	30	2.86	3.54	15.80	12.00	1.96	2.27	11.47	18.33
4	6	30	2.11	2.58	17.99	9.50	2.04	2.47	11.17	12.50
12	4	50	1.94	2.45	11.64	11.00	1.92	2.35	10.43	13.33
4	2	30	2.24	2.79	12.09	3.00	1.91	2.36	10.99	4.17
8	2	10	3.01	3.69	17.52	3.50	2.87	3.56	16.55	5.12
12	6	30	2.03	2.57	12.09	27.33	2.01	2.63	12.39	34.50
8	6	50	2.05	2.56	11.91	13.50	1.91	2.38	11.63	13.33
8	2	50	1.99	2.55	13.42	5.50	1.61	2.01	9.61	7.37
8	4	30	1.80	2.24	9.90	14.50	2.16	2.35	11.67	20.86
8	6	10	2.52	3.11	14.32	21.00	2.43	3.08	15.00	45.00
12	2	30	2.67	3.22	13.98	7.50	2.55	3.19	14.01	9.17
12	4	10	2.49	3.04	13.68	25.00	2.36	3.02	14.11	32.50
8	4	30	2.42	2.97	14.60	14.00	2.06	2.17	11.66	19.56

$$\text{Rz DI water} = 12.00 + 1.31\,A + 0.15\,B - 0.112C - 0.0429\,A \times A + 0.194\,B \times B - 0.00084C \times C - 0.234\,A \times B + 0.0062\,A \times C + 0.0063\,B \times C \quad (4)$$

Regression equations for MRR, Ra, Rq and Rz for the dielectric with nanosheets in Uncoded units

$$\text{MRR Graphene} = -47.1 + 4.86\,A + 9.05\,B + 1.110C - 0.2198\,A \times A - 0.247\,B \times B - 0.00224C \times C + 0.531\,A \times B - 0.0551\,A \times C - 0.2120\,B \times C \quad (5)$$

$$\text{Ra Graphene} = 3.091 + 0.1231\,A - 0.341\,B - 0.0486C - 0.00120\,A \times A + 0.0418\,B \times B + 0.000149C \times C - 0.02084\,A \times B + 0.000459\,A \times C + 0.00461\,B \times C \quad (6)$$

$$\text{Rq Graohene} = 4.691 + 0.048\,A - 0.671\,B - 0.0735C + 0.00584\,A \times A + 0.0820\,B \times B + 0.000500C \times C - 0.0227\,A \times B - 0.00003\,A \times C + 0.00534\,B \times C \quad (7)$$

And,

$$\text{Rz Graphene} = 21.55 + 0.451\,A - 2.756\,B - 0.3724C - 0.0095\,A \times A + 0.295\,B \times B + 0.00203C \times C - 0.0656\,A \times B + 0.00439\,A \times C + 0.02652\,B \times C \quad (8)$$

3.1. Effect of dielectric medium with nanosheets and without nanosheets on MRR

Fig. 1 illustrates the impact of the dielectric medium, both with and without nanosheets, on the MRR. The interaction plot presented in Fig. 1 demonstrates the relationship between process parameters and response parameters. Here, Ip, Ton and Gv and Ip_P, Ton_P and Gv_P indicates responses without graphene powder (curves with dash line), and with graphene powder (curves with continuous line) respectively. In Fig. 1 (a), it is evident that increasing the pulse on time while maintaining a constant gap voltage of 30V leads to an increase in MRR, which further escalates with higher peak current. Notably, the introduction of nanosheets into the dielectric medium results in a higher MRR at increased peak current and pulse duration [57–59]. A similar observation is depicted in Fig. 1(c), where the maximum MRR is achieved at higher peak current and a 10V gap voltage. The trend displayed in Fig. 1(c) indicates a decreasing order of MRR with increasing gap voltage, all while maintaining a constant peak current of 4A. This decrease in MRR can be attributed to the enlargement of the plasma channel during the machining process, resulting from a higher spark gap. Consequently, the discharge energy per unit area decreases, thereby influencing the MRR [57,60,61].

3.2. Effect of dielectric medium with nanosheets and without nanosheets on surface roughness (Ra, Rq and Rz)

The surface roughness obtained from the experiments is plotted in the form of the input parameters' interactions in Fig. 2, Fig. 3, and Fig. 4. Also here, Ip, Ton and Gv and Ip_P, Ton_P and Gv_P indicates responses without graphene powder (curves with dash line) and with graphene powder (curves with continuous line) respectively. The graphene nanosheets (conductive) in the dielectric medium observed a

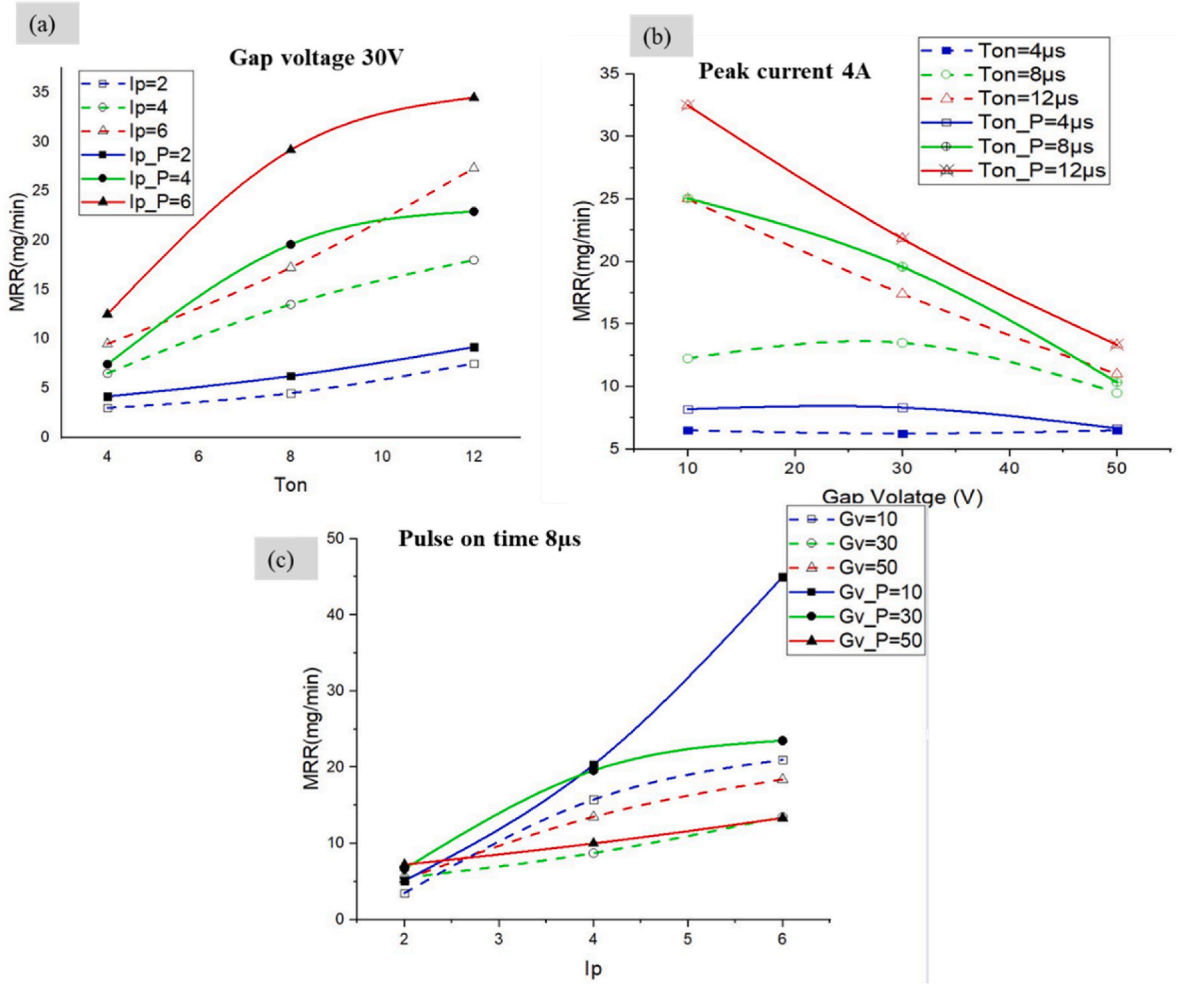

Fig. 1. Relationship between input and output parameters for MRR responses [curves with dash line is illustrating the without graphene powder, while, the curves with continuous line is illustrating with graphene powder].

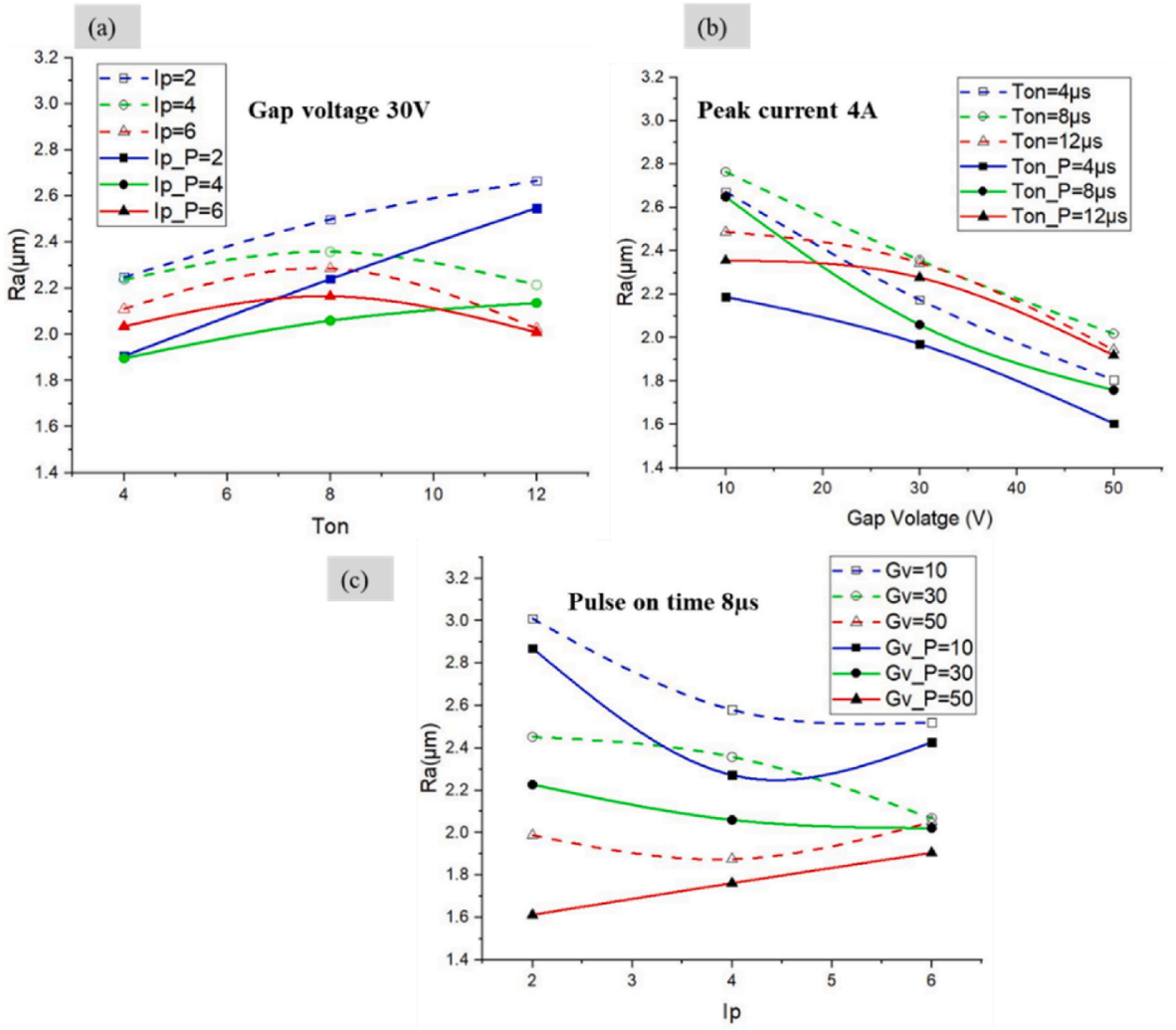

Fig. 2. Relationship between input and output parameters for Ra [curves with dash line is illustrating the without graphene powder, while, the curves with continuous line is illustrating with graphene powder].

considerable decrease in roughness [62–64]. The plasma channel formation gets modified due to the presence of nanosheets between the tool and the workpiece. It gets enlarged. The nanosheet discrete the single spark into multiple sparks and discharges energy distributed over a large surface area [65–67]. As a result, shallow craters formed over the machined surface [5] The plasma channel does not press heavily to the molten metal, which avoids the gases' entrapment into the cavity, making it less defective. Thus, the machined surface became uniform, smooth and less concave [36,57].

3.3. Debris analysis

The collection of workpiece debris occurs post-machining. The dielectric medium, containing residue, is left uncovered in an open environment for 1 h, with the beaker's top covered by aluminum foil. After this duration, deionised water is poured, allowing settled debris particles to be collected. Subsequently, the collected debris is dried in an oven at 80 °C for 4 h, followed by 120 °C for 3 h. The dried debris is then subjected to particle size analysis [68–70]. The results, as depicted in Fig. 5, demonstrate that the debris produced in NSMEDM is smaller compared to conventional EDM. In NSMEDM, the maximum debris percentage ranges between 10 and 100 μm, whereas in traditional EDM, the maximum percentage of debris falls within the range of 100–1000 μm. It is noteworthy that the size of debris particles is smaller when operating at lower discharge energy, and vice versa [71–73]. The challenge lies in avoiding particle agglomeration, as it leads to an increase in the size of debris particles [74,75]. Fig. 5 reveals the smaller size of debris produced during machining in NSMEDM when compared to the use of deionised water as the dielectric medium.

Transmission Electron Microscopy (TEM) analysis is done to observe the size of a single debris particle. Figs. 6 and 7 show the particles produced in deionised water and graphene nanosheets mixed dielectric mediums. Figs. 6(a) and 7(a) show debris particles' agglomeration. EDX is done to confirm that the debris particle is the same as the parent material [76–78]. Single debris particle size is measured, 996.27 and 514.13 nm in deionised water and graphene nanosheets mixed dielectric.

3.4. Phase analysis

The machined surface layer XRD pattern was obtained using Rigaku (Model- Smartlab) XRD. X-ray diffraction (XRD) identifies the measured phase present on the surface. The diffraction was measured from 20° to 150°, a step of 0.055°, and analysed using X'Pert HighScore Plus software. Fig. 8 manifests the XRD patterns for Inconel 718 base metal and machined surfaces at 8μs, 2A and 50V. The peaks show the compound present in the materials with crystal shape and size. The compound found in base metal (Inconel 718) is Cu0.81Ni0.19, Cr0.19Fe0.70Ni0.11 and $Cu_{3.8}Ni$, having a Cubic crystal structure. The machined surface obtained using only deionised water has a similar compound as base

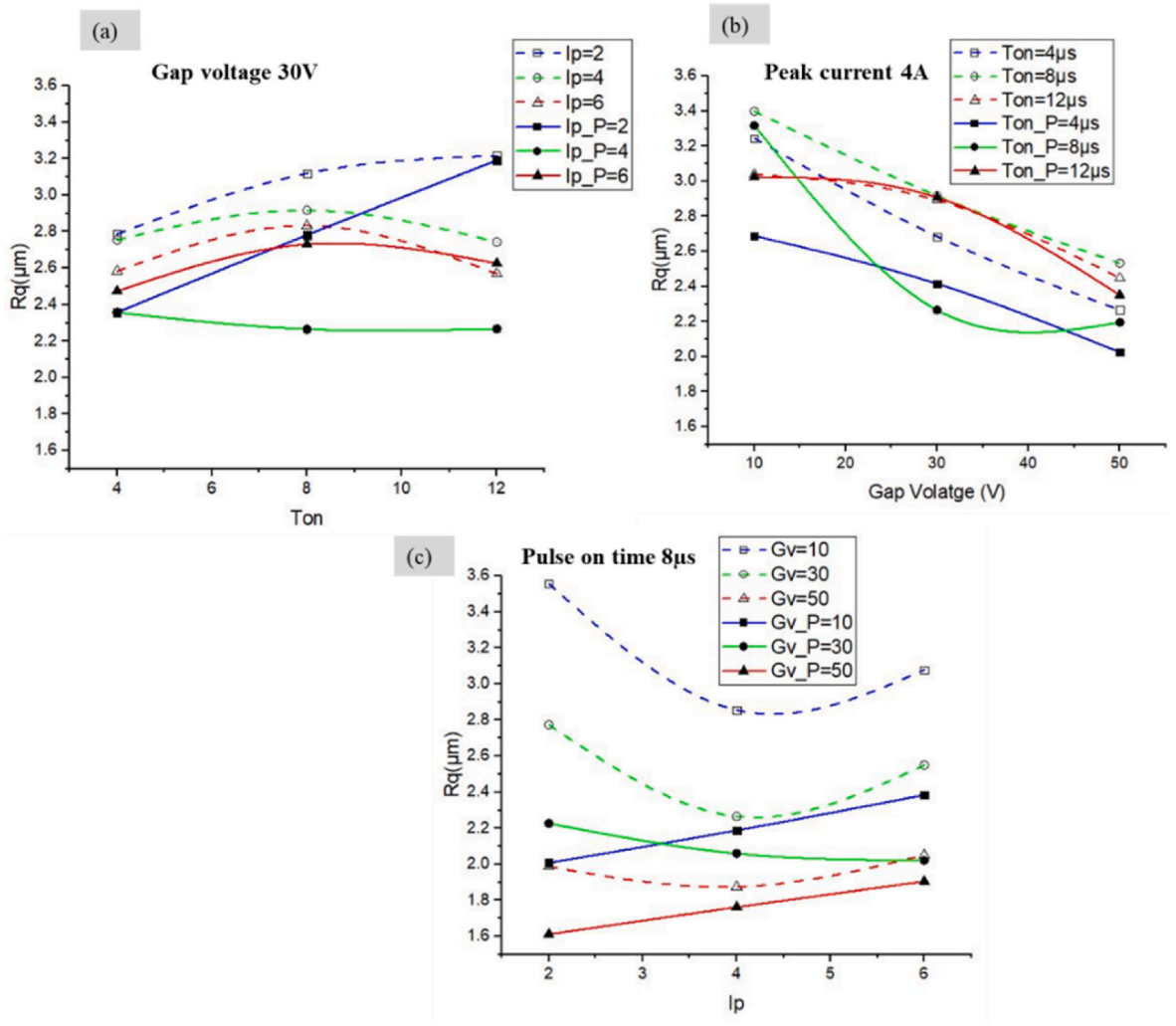

Fig. 3. Relationship between input and output parameters for Rq [curves with dash line is illustrating the without graphene powder, while, the curves with continuous line is illustrating with graphene powder].

metal, adding some oxide and pure elements [79–81]. The compounds are $Cu_{0.81}Ni_{0.19}$, $Fe_{0.64}Ni_{0.36}$, Fe0.64Ni0.36 and Ni–Cr–Co–Mo. The machined surface obtained using graphene nanosheets in deionised water shows the same compounds as the parent material ($Cu_{0.81}Ni_{0.19}$, $Cr_{0.19}Fe_{0.70}Ni_{0.11}$, $Fe_{0.64}Ni_{0.36}$). The presence of Cu on the metal surface shows the consumption and erosion of the Cu electrode [82–84]. This phenomenon has also been examined by Refs. [59,60]. There is no significant change in compound formation detected. The crystallite size of the elements was also calculated from the XRD data. Ni, Cu, Cr and Fe have crystallite sizes of 17.54, 17.36, 28.38 and 22.52 nm.

3.5. Residual stresses

Residual stresses are generated over the machined surface in EDM, which is measured using Riguku, a multipurpose high-resolution x-ray diffractometer (HRXRD) instrument. During the machining process, heating and cooling of the workpiece, expansion, and contraction occur, resulting in residual stress on the machined surface [85–87]. The presence of the dielectric medium behaves as a quenching medium. Also, plastic deformation occurs due to non-homogeneity in heat flow during solidification [88]. The sparking phenomenon in the EDM process develops extreme temperature differences over the machined surface [89–91]. Rapid heating and cooling during the machining process produce tensile residual stresses on the EDMed surface [61]. Residual stress observed for base material (Inconel 718) is -4887.99 ± 4779.55 MPa at (2θ at $\psi = 0°$:138.28 ± 2.770), which is compressive. Minimum residual stresses in NSMEDM and conventional EDM are -113.29 MPa and 110.97 MPa. Besides, the maximum residual stresses are 530.61 MPa and 851.67 MPa at (2θ at $\psi = 0°$:138.871 ± 0.210) and at (2θ at $\psi = 0°$:137.69 ± 0.187), respectively as shown in Fig. 9. The residual stress was reduced with nanosheets addition into the dielectric medium because of the spark gap's enlargement, which reduced the discharge energy density [61]. Therefore, the minimum and maximum improvement in residual stresses is calculated, 224.26 MPa and 321.06 MPa, respectively.

3.6. Surface modification

The surface modification takes place due to the resolidification of the molten metal [92,93]. When the material resolidifies, the unflushed debris components and nanosheets in the dielectric get adhered to the molten metal and sometimes mixed into the molten, forming another compound [94–96]. In this investigation, the surface modification is analysed by composition testing on Zeiss, Germany. It has an attachment for EDX analysis, Fig. 10. The EDS analysis confirms the transfer of external material to the machined surface [97–99]. The Cu composition of the base material increases from 1.21 to 4–6 wt%. On different machining conditions, as shown in Table 6. The carbon wt% increases from 0.45 to 2–4 wt% in the conventional EDM process. However, when nanosheets mixed dielectric is used, many carbon elements are observed

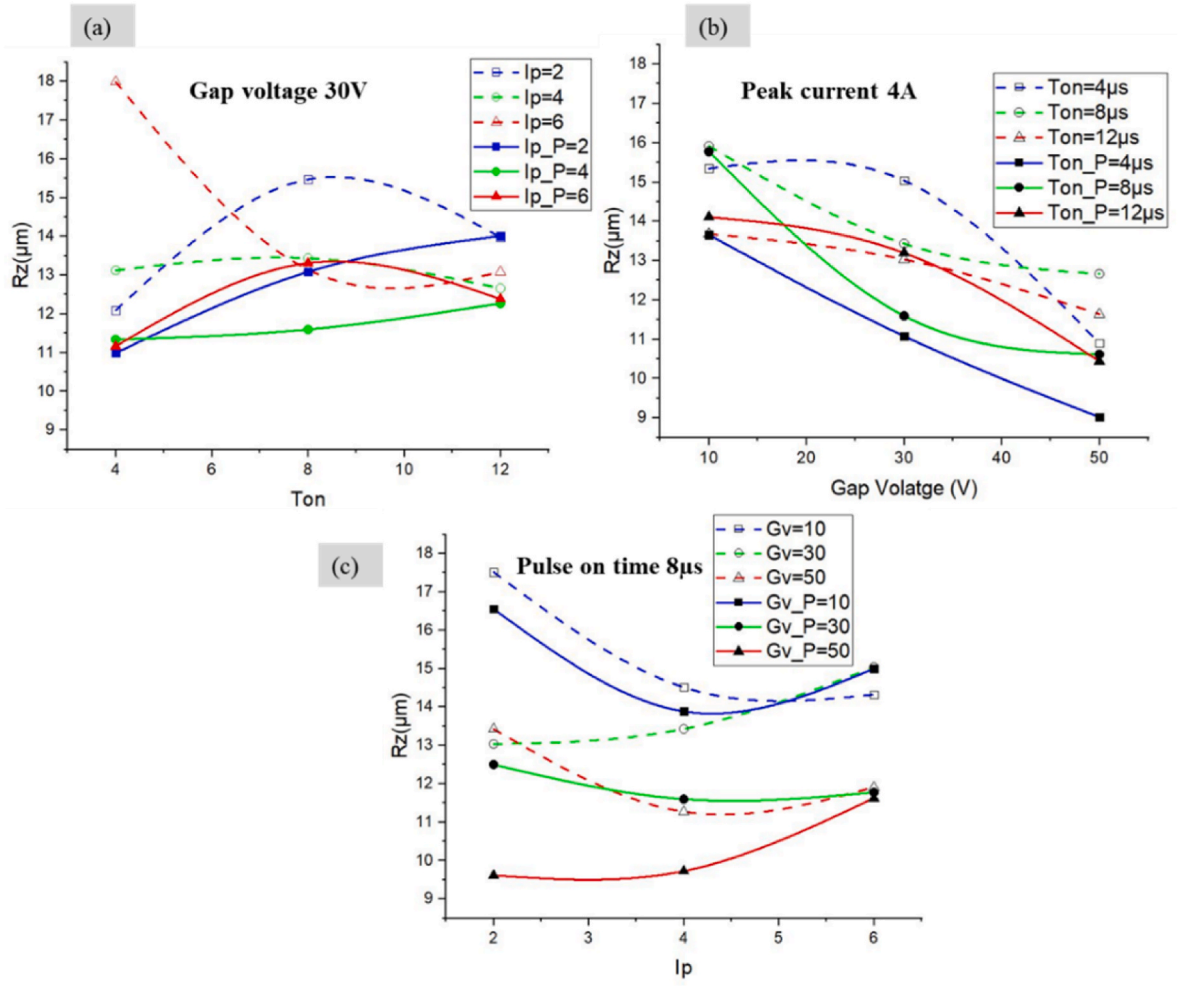

Fig. 4. Relationship between input and output parameters for Rz.

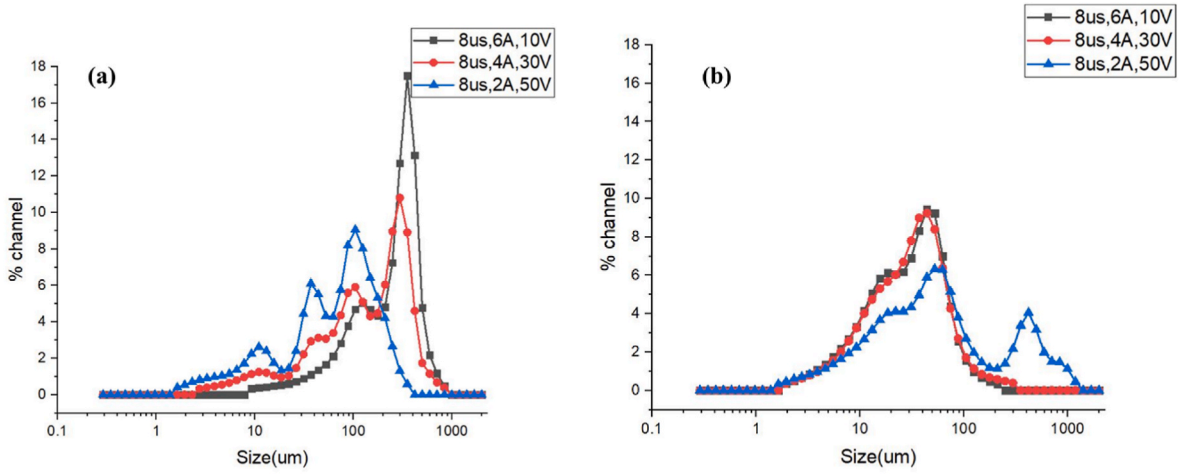

Fig. 5. Debris particle size in the dielectric medium (a) deionised water and (b) deionised water with graphene nanosheets.

at approximately 10–14 wt% over the machined surface [100–102]. This phenomenon changes the properties of the surface layer. The hardness of the machined surface also increases after the EDM process shown in Fig. 11. The hardness of the redeposited materials over the machined is about 32.64 % higher than the base material due to rapid heating and quenching in the deionised dielectric medium [62,63]. Besides, the hardness increases by 100.4 % in graphene nanosheets mixed dielectric medium due to the inclusion of carbon particles into the molten material [103–105].

3.7. Deposited materials, globules and micro-holes

The microstructure of the machined surface has been observed through FESEM at 2000× magnification. The machined surfaces shown

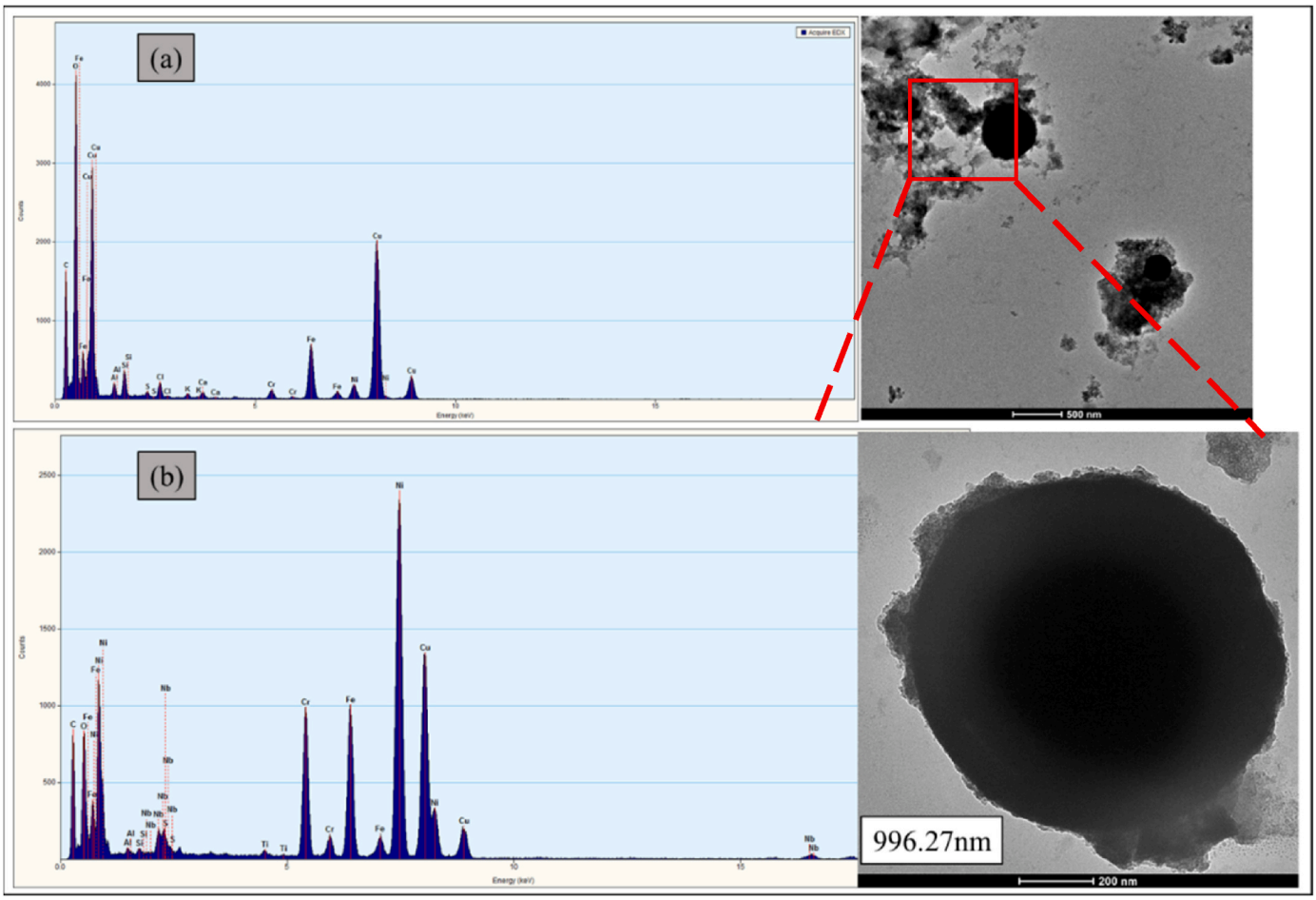

Fig. 6. (a) and (b) TEM analysis of debris particles in case of deionised water at 8μs, 2A and 50V.

in Fig. 12 depict the deposited materials over the machined surfaces, including microholes and globules. There are no microcracks found over the machined surface. When machining the workpiece through the EDM process in a deionised water dielectric medium, a high amount of molten material deposition is observed and depicted in Figs. 12(a) and 10(c) [106–108]. This is because of the high discharge and short spark gap; High discharge energy melts a high amount of material, whereas an insufficient spark gap prevents the flushing from flushing out all the molten material from the machining region [109–111]. Hence high deposition takes place over the machined surface. When nanosheets mixed dielectric is used as a dielectric medium, a small amount of molten metal deposition occurs due to low discharge and sufficient large spark [112,113]. Fig. 12(b and d) depicts the deposition of molten metal during NSMEDM. The EDM process has temperatures ranging from 8000 to 12000 °C, enough to melt and evaporate Inconel 718. But the exploding pressure is insufficient to remove all the molten material from the machined surface, and the molten material splashes over the machined surface [64]. The splashed material is resolidified over the machined surface and is called deposited material [114,115]. The formation of the globules is similar to powder production through the atomisation process [65]. During the machining, a high volume of gas is supersaturated in the plasma channel [116,117].

Therefore, when molten metal is resolidified over the machined surface, some air bubbles are entrapped into the molten metal, forming a microhole over the machined surface [118]. A high amount of molten metal produces large microholes over the machined surface at high discharge energy [119]. Fig. 13(a and b) show the large and small microholes at 8 μs, 6A and 10V and 8 μs, 2A and 50V in conventional EDM. In NSMEDM Fig. 13(c and d), discharge energy was reduced drastically. Therefore, tiny micro holes are observed at 8 μs, 6A, and 10V while the machined surface at 8 μs, 2A and 50V is microhole free.

The surface texture of the machined surface was examined at a high magnification of 15,000×. There are nonuniform-deposited materials all over the machined surface and improper machining marks. It shows an uneven surface formed over the machined surface due to irregular deposition of the debris particles when using the conventional EDM process, as shown in Fig. 14(a and c). It is because of improper flushing due to the low spark gap and high discharge energy [120]. A smooth surface was obtained using the NSMEDM process, as shown in Fig. 14(b and d). When Nanosheets are mixed into the dielectric medium, it reduces its resistivity, enlarging the spark gap. Thus, a large and wide plasma channel has a sufficient spark gap between flushing out most debris particles and producing smooth surfaces [121]. Fig. 13 shows that in the case of deionised water at 8 μs, 2A and 50V, pin type structure formed over the machined surface, whereas in NSMEDM, the smooth surface is formed. It is due to the flushing of molten metal from the machined zone [122–124].

3.8. Recast layer thickness

The EDM process generates extremely high temperatures at the point of electrical discharge. This causes localised melting and vaporization of the workpiece material. When the molten material solidifies rapidly, it forms a layer on the machined surface known as the surface white layer. The thickness and properties of this layer depend on various factors, including the EDM parameters, workpiece material, and electrode material. It enhances wear resistance and improved surface finish by acting as a self-polishing mechanism [125,126]. It also the main cause of

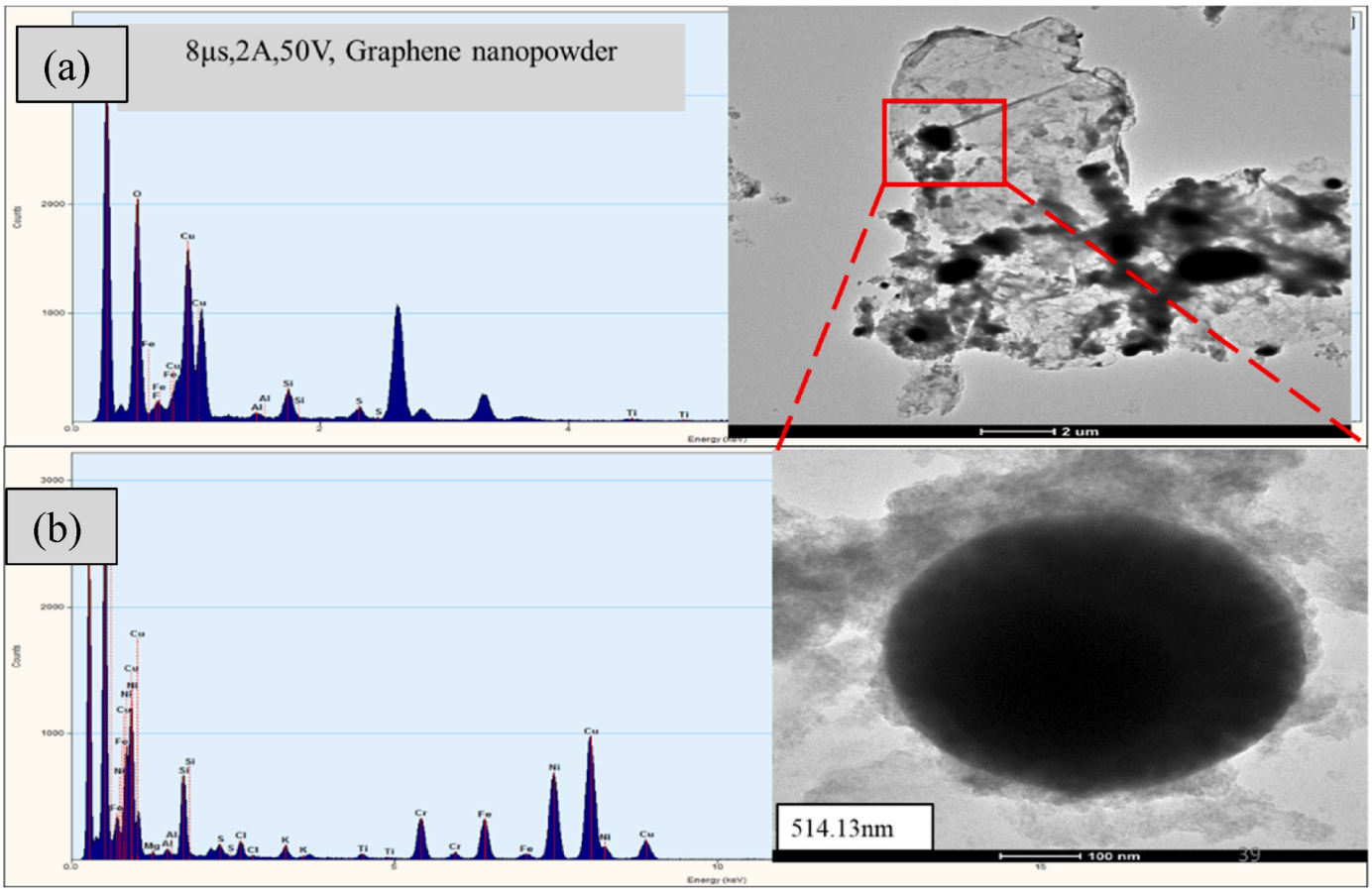

Fig. 7(a). and (b) TEM analysis of debris particles in the case of graphene nanosheets at 8µs, 2A and 50V.

residual stresses, reduced fatigue life, reduced materials properties and in some cases increases surface roughness [65]. Additionally, the formation of the surface white layer throughout both NSMEDM, and EDM has been attributed to the considerable heat generated during the discharge process. Material that is located at close vicinity to the surface encounters an action of melting followed by speedy cooling, leading to an altered microstructure. Furthermore, the NSMEDM exhibits reduced discharge energy, which enables a more precise, and appropriately controlled application of heat-input in a localised manner. Consequently, the utilisation of this technique leads to a reduced thickness as well as minimal structural modification of the surface's white layer in comparison to traditional EDM methods [127].

In order to examine the recast layer thickness under a FESEM, the sample is cut in a transverse direction using wire EDM (WEDM). Subsequently, the cut surface is polished using emery paper with grit sizes of 800, 1000, 1200, 1500, and 2000, followed by a final polish using diamond paste on a velvet polishing cloth. During diamond polishing, an aerosol lubricant is used instead of water. However, in order to visualize the recast layer thickness, an etching process is necessary for the samples [128]. The etchant solution is prepared by mixing 15 ml of HCl, 10 ml of HNO_3, 10 ml of acetic acid, and 2–3 drops of glycerol, and the samples are immersed in the solution for 30–45 s. Fig. 15 exhibits the transverse cut samples of the machined surface at a magnification of 2000×. The figure demonstrates that NSMEDM results in a thinner recast layer compared to conventional EDM. Specifically, at 8 µs, 2A, and 50V, the recast layer thickness in conventional EDM measures 11.46 µm and 12.48 µm, while in NSMEDM, it measures 2.93 µm and 4.45 µm. This signifies a reduction of 74.43 and 64.34 % in the recast layer using NSMEDM under the mentioned conditions [129]. At times, differentiating the recast layer from the base material can be challenging, necessitating higher magnification to observe the cross-section part. Fig. 16 showcases the microstructure of the base material and the recast layer at a magnification of 60,000×. The microstructure of the recast layer reveals the formation of multiple layers resulting from the resolidification of the molten metal, while the base metal's microstructure appears smooth and uniform [128,130].

The surface morphology analysis was conducted utilizing a Zeiss-made FESEM at IIT (ISM) Dhanbad. The FESEM's high-resolution magnification capability enabled a detailed investigation of the surface morphology at the micro-level [131]. To prepare the sample for analysis, cutting through WEDM was employed. Additionally, polishing was carried out on the sectioned part using polishing papers of varying grit sizes, facilitating the measurement of the recast layer thickness (RCL).

As far as the comparative-analysis with existing studies are concerned, one of the studies by Muthuramalingam (2019) has aimed to investigate the EDM process applied to AISI 202 stainless steel (SS) with the following objectives, the objective of the study is to investigate the influence of pulse generators on the development of a white layer in the EDM process [67]. The objective of their study was to examine the impact of numerous process-operating variables on the "Average White Layer Thickness" (AVLT) in EDM [67].

The "iso energy pulse-generator" (IPG) has been observed to produce a smaller white layer with uniform thickness levels. The observed outcome can be attributed to the capability of the system to offer reduced and uniformly dispersed spark energy. On the other hand, the "transistor conventional pulse-generator" (TPG) generates varying quantities of thicker AVLT. It is noteworthy to highlight that the composition structure and formulation content of the white layer is subject to impact caused by the resolidification of molten material originating from both the workpiece and the electrode. The physical characteristics of the tool electrode also contribute to the determination

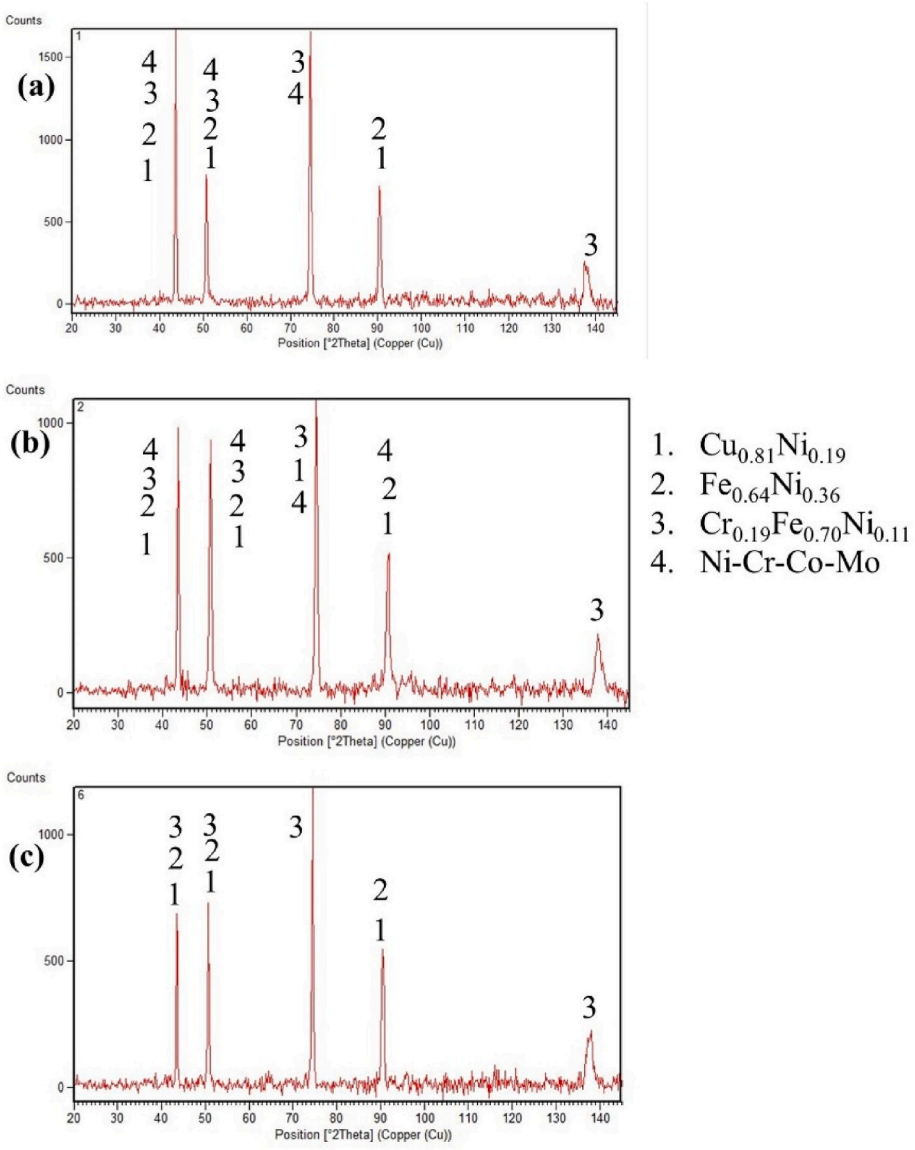

Fig. 8. The XRD patterns of the base metal and the EDMed surface layer (a) Base Metal, (b) Without nanosheets and (c) With nanosheets at (T_{on} 08 μs, Toff 17.5 μs, 2A, and 50V).

of AVLT. W carbide electrodes, by virtue of their raised melting point relative to stainless steel, have a propensity to yield reduced AVLT. Conversely, the utilisation of brass tool electrodes, characterised by their comparatively lower melting point, leads to elevated AVLT, and enhanced surface roughness [67].

The IPG has a consistent capability to produce a thin white-layer coating on the machined surface owing to its evenly homogenous distribution of spark energy, hence ensuring a consistent duration of discharge current throughout the machining spark discharges [67].

On the other hand, the TPG exhibits an enhanced ability to generate raised spark energy through a randomised dispersion, contributing to raised variability and increased white layer thickness [67].

In structures subjected to bending stresses, it is observed that the topmost layer of the workpiece undergoes the highest level of strain as unveiled by Klocke et al. (2016) [68]. The characteristics of this layer are of utmost significance for the overall mechanical functionality of the component. Within the realm of WEDM process, the machining process is influenced by the thermal material loading and modification of the surface layer [68].

The WEDM method is distinguished by its utilisation of a thermal material removal principle, which leads to a discernible modification of the rim zone [68]. This change notably includes the formation of an exterior shell often known as the “white layer.” Although the impact of this white layer on mechanical durability is typically reduced, its specific structure and content still remain uncertain. It is significant to comprehend the characteristics of this white layer, since it has a substantial impact on the mechanical characteristics of the workpiece [68].

In order to conduct a thorough examination of the aforementioned layer, the composition of the rim zone is analysed using chemical techniques, in conjunction with the utilisation of TEM photographs, to ascertain its microstructural composition [68]. The study examines the impact of localised imperfections and transitions on the performance of the workpiece. The chemical composition of the white layer is determined through the use of both EDX-maps and standard EDX investigations. Furthermore, nanoindentation-based mechanical testing techniques are employed to quantify the localised hardness and modulus of elasticity inside the white layer. The quantification of the impact of edge geometry may be achieved by a comparative evaluation of the local hardness and modulus of elasticity among the altered rim zone and an unaffected surfaces layer [68].

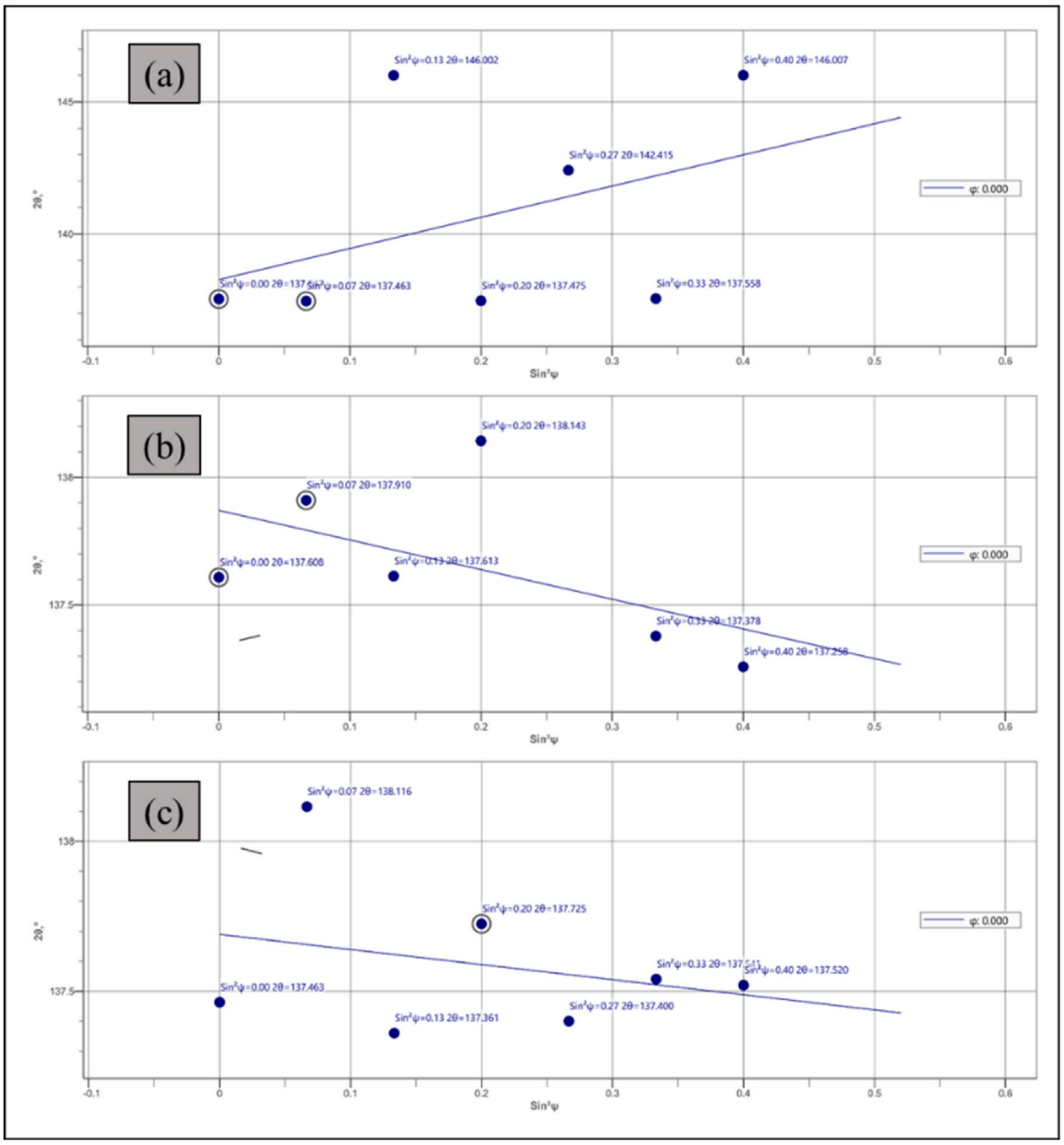

Fig. 9. Residual stresses present in (a) Base metal and machined surface at 8μs, 2A and 50V using the dielectric medium, (b) deionised water and (c) graphene nanosheets mixed.

The exhaustive study conducted allows for a thorough evaluation of the chemical composition and metallurgical constitution of the white layer, which predominantly governs its mechanical characteristics [68]. This insight enables the anticipation of the mechanical characteristics demonstrated by workpieces that have undergone WEDM machining, especially for components that possess significant differences in higher aspect-ratios, and complex geometries [68].

In brief, the aim of the study was to analyze the chemical composition, structure, and mechanical characteristics of the white layer formed during the fine machining procedure of WEDM [68]. The subsequent significant discoveries were acquired, the chemical study conducted indicated that the white layer comprises components originating from the wire electrode, namely Cu and zinc, as well as molybdenum derived from the carbides prevalent in the molten parent material. The existence of vanadium and chromium was not apparent in the white layer [68].

The metallurgical investigation conducted employing TEM revealed that the white layer mostly displays an amorphous microstructure [68]. However, it undergoes a transition to crystalline structures at the interface with the parent material [68].

The findings of local hardness measurements revealed a substantial augmentation in hardness inside the recast layer, exhibiting an almost double rise in comparison to the hardness of the original material [68]. The impact associated with the geometric characteristics of the workpiece edge was alleviated.

The examination for the modulus of elasticity in the white layer, when compared to an unaffected surface, indicated no substantial changes in Young's modulus. The relatively small discrepancies observed in close proximity to the surface were ascribed to the presence of a nickel support layer [68].

It is crucial to acknowledge that several elements pertaining to the characteristics of the recast layer were not comprehensively assessed, namely with regards to carbon contamination and the dispersion of

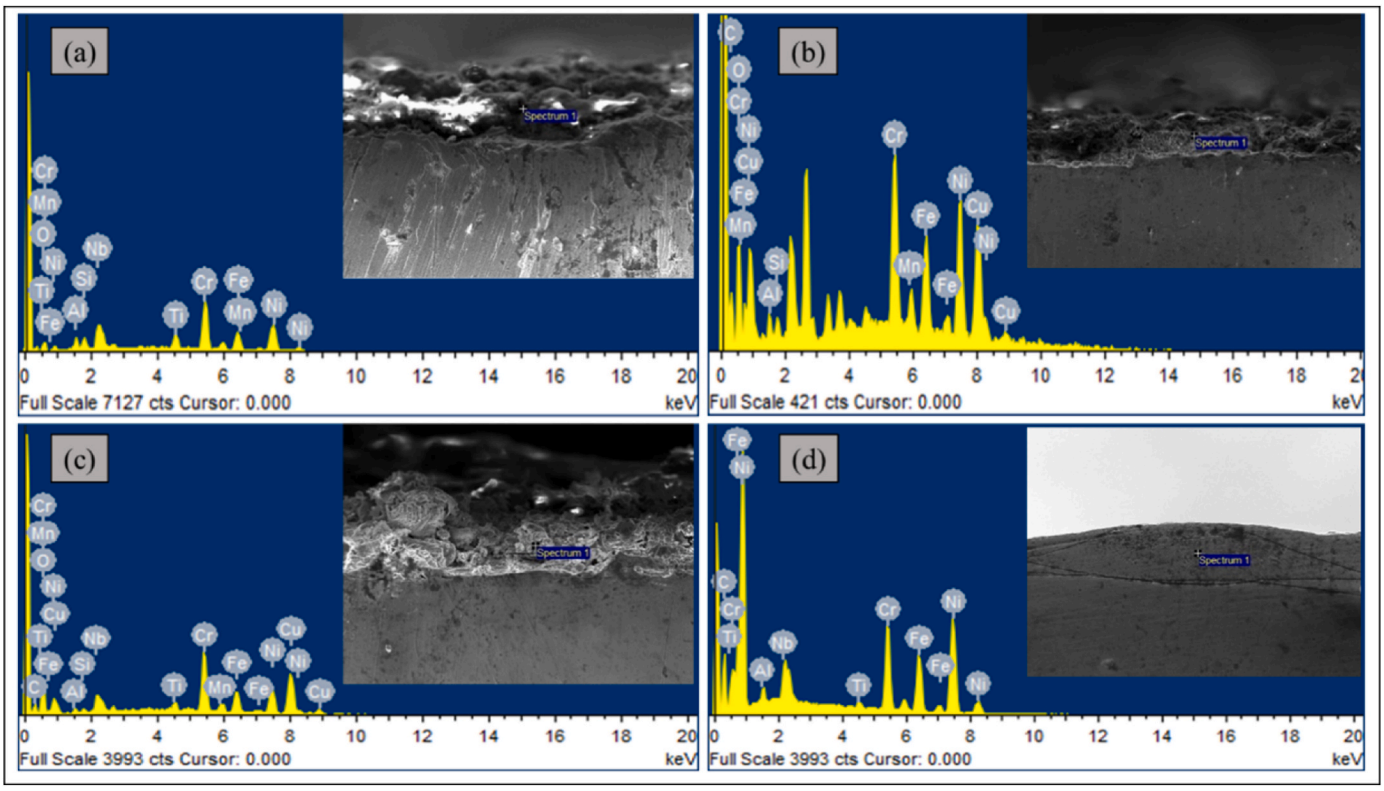

Fig. 10. Energy-dispersive x-ray spectroscopy analysis images; (a) conventional EDM at 8 μs, 2A and 50V, (b) NSMEDM at 8 μs, 2A and 50V (c) conventional EDM at 8 μs, 6A and 10V, (b) NSMEDM at 8 μs, 6A and 10V.

Table 6
Elemental composition of machined surface at the different machining conditions.

Elements	C K	O K	Al K	Si K	Mo K	Ti K	Cr K	Mn K	Fe K	Ni K	Nb L	Cu L
Base Material	0.45	3.32	0.95	0.67	3.12	1.32	17.15	1.56	19.31	46.69	4.25	1.21
8μs,2A,50V DI water	2.35	3.71	1.42	1.87	2.89	3.92	23.15	2.34	12.41	33.62	7.84	4.48
8μ,2A,50V Graphene	10.32	6.24	0.98	0.63	3.15	0.87	15.02	3.56	11.28	36.14	5.35	6.46
8μs,6A,10V DI water	3.99	7.43	0.78	0.52	2.99	2.49	24.26	2.15	13.52	30.24	6.15	5.48
8μs,6A,10V Graphene	13.47	6.72	0.82	0.76	2.25	0.81	14.53	2.65	13.78	34.78	3.93	5.81

residual stress within the white layer [67].

The intent of the investigation was to assess the machinability of Inconel 718 through the utilisation of EDM employing a dielectric medium mixed with Gr powder [69]. The analysis took into account numerous process-performance characteristics, such as material removal efficiency, tool wear rate, and surface quality. A comprehensive analysis was performed on the machined surface, whereby several parameters including roughness, fracture density, white layer depth, residual stress, and microhardness were investigated. The obtained findings were afterwards compared with those generated by standard EDM techniques [69].

Furthermore, our study encompassed an examination of material migration, the development of intermetallic compounds, the refinement of grain structure, and several other metallurgical variables that are impacted by the EDM process [69]. This research also encompassed a quantitative assessment of the metallurgical characteristics of the machined surface, specifically focusing on variables such as crystallite size, microstrain, dislocation density, and their respective fluctuations resulting from the thermomechanical impacts of EDM [69].

In summary, the findings of the study highlighted notable disparities among PMEDM and traditional EDM [69]. The application of PMEDM led to the formation of a more substantial white layer as a consequence of the presence of consecutive discharge sparks. This phenomenon contributed to an enhancement in the efficiency of material removal, albeit in spite of a raised production of debris on the surface being worked with. The accumulation of debris on the machined surface and the formation of a deeper white layer were considerably impeded by the presence of powder particles that were agglomerated locally inside the dielectric medium [69].

Moreover, it was discovered that the microhardness values for all specimens subjected to EDM were higher than those of the original material [69]. This can be attributed to the development of carbide layers with high hardness and low conductivity on the surface of the machined specimens. The dispersion of carbide layers inside the white layer had an impact on the microhardness tests conducted at a spot roughly mid-depth through the white layer. The rise of peak current resulted in an increase of energy input, hence leading to an escalation of thermal stress. When the heat stress exceeded the ultimate tensile strength of the surface that underwent EDM, fractures were developed and propagate through the white layer and into the parent material, resulting in further erosion of the material [69].

The inadequate efficacy of the dielectric fluid in eliminating debris from the machined area resulted in the re-solidification of molten material, resulting in the formation of a progressively thicker white coating as the discharge current steadily increased [69]. In the context of PMEDM, the inclusion of Gr particles, due to their high thermal

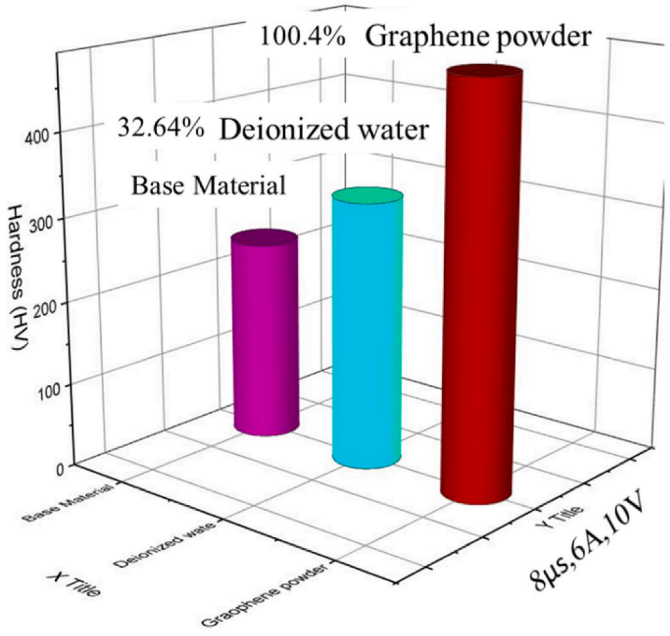

Fig. 11. Vickers hardness of base material, machined surface through conventional EDM and NSMEDM.

conductivity, facilitated the dissipation of heat energy during the discharge process, hence leading to the development of a comparatively thicker white layer. Nonetheless, the accumulation of excess powder in close proximity to the gap nearest to the machined surface impeded the removal of debris, leading to a prolonged period of solidification and the formation of a more substantial white layer. However, a subset of the specimens demonstrated a higher density and reduced thickness of the white coating in comparison with conventional EDM methods [69].

Another comparable study by Ekmekci (2007), where research was undertaken to investigate the impact of dielectric liquid choice and electrode type on the morphology of the white layer formed on surfaces subjected to EDM [70]. The study primarily centred on the investigation of retained austenite and residual stresses through the utilisation of XRD analysis. The machining tests were conducted using two distinct tool electrodes, namely Cu and Gr, together with two dielectric liquids, specifically kerosene and de-ionized water. These experiments were performed under similar operational conditions. The outcomes of this research indicate the following main findings, when performing machining processes utilizing a dielectric liquid composed of hydrocarbons, such as kerosene, it has been discovered that the resulting machined surface gets saturated with carbon, irrespective of the material employed as the tool electrode. Nevertheless, the amount of carbides within the white layer could vary as a consequence of the supplementary carbon introduced by the electrode material [70].

The carbon provided by the tool electrode offers a crucial function in the formation of the austenite phase within the white layer during machining, particularly when de-ionized water is employed as the dielectric liquid [70–72].

The magnitude of surface residual stresses correlates favorably with the degree of structural non-homogeneities present inside the white layer. The forces experienced might exceed the fracture strength of the material, which leads to the occurrence of microcracks that are randomly distributed over the machined surface [70,73,74].

The impact of residual stresses resulting from phase transformations occurring inside the white layer is relatively minimal in terms of their

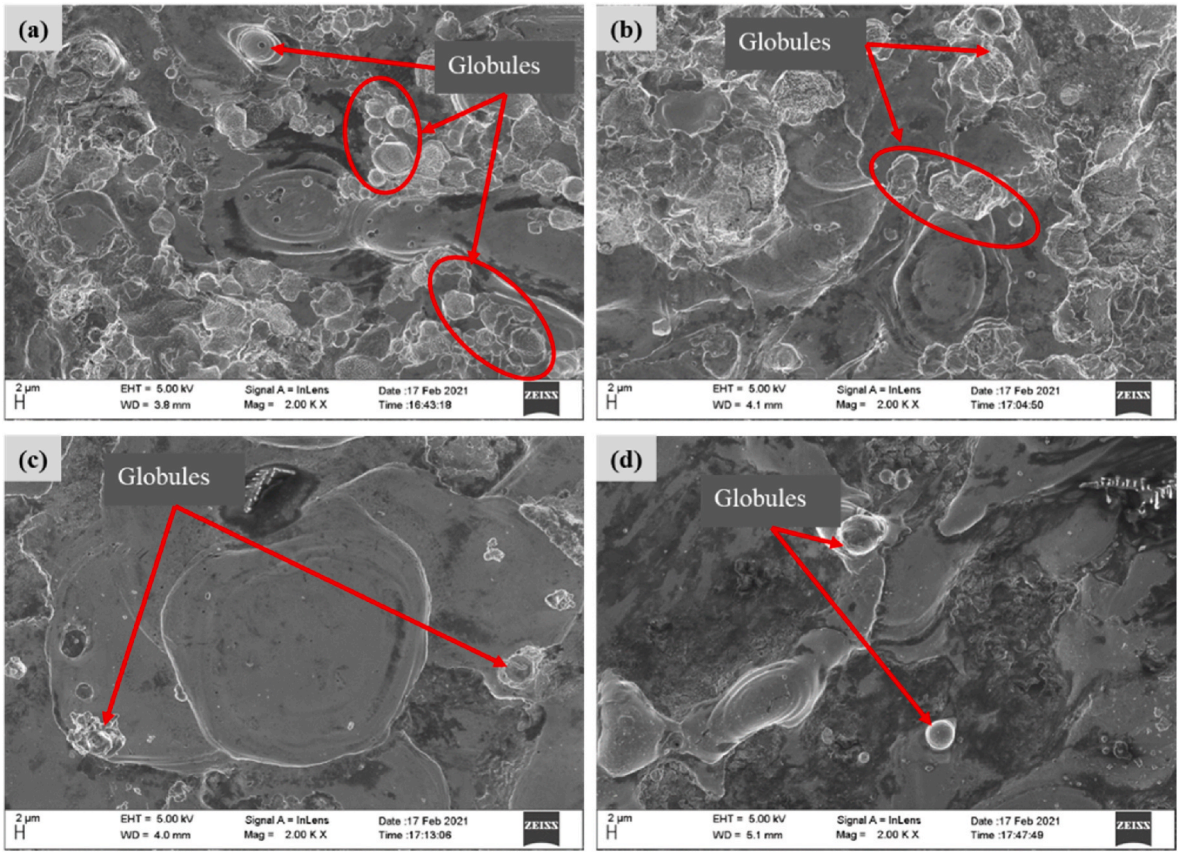

Fig. 12. FESEM image of machined surface at the following conditions: (a) conventional EDM at 8 µs, 2A and 50V, (b) NSMEDM at 8 µs, 2A and 50V, (c) conventional EDM at 8 µs, 6A and 10V, (b) NSMEDM at 8 µs, 6A and 10V.

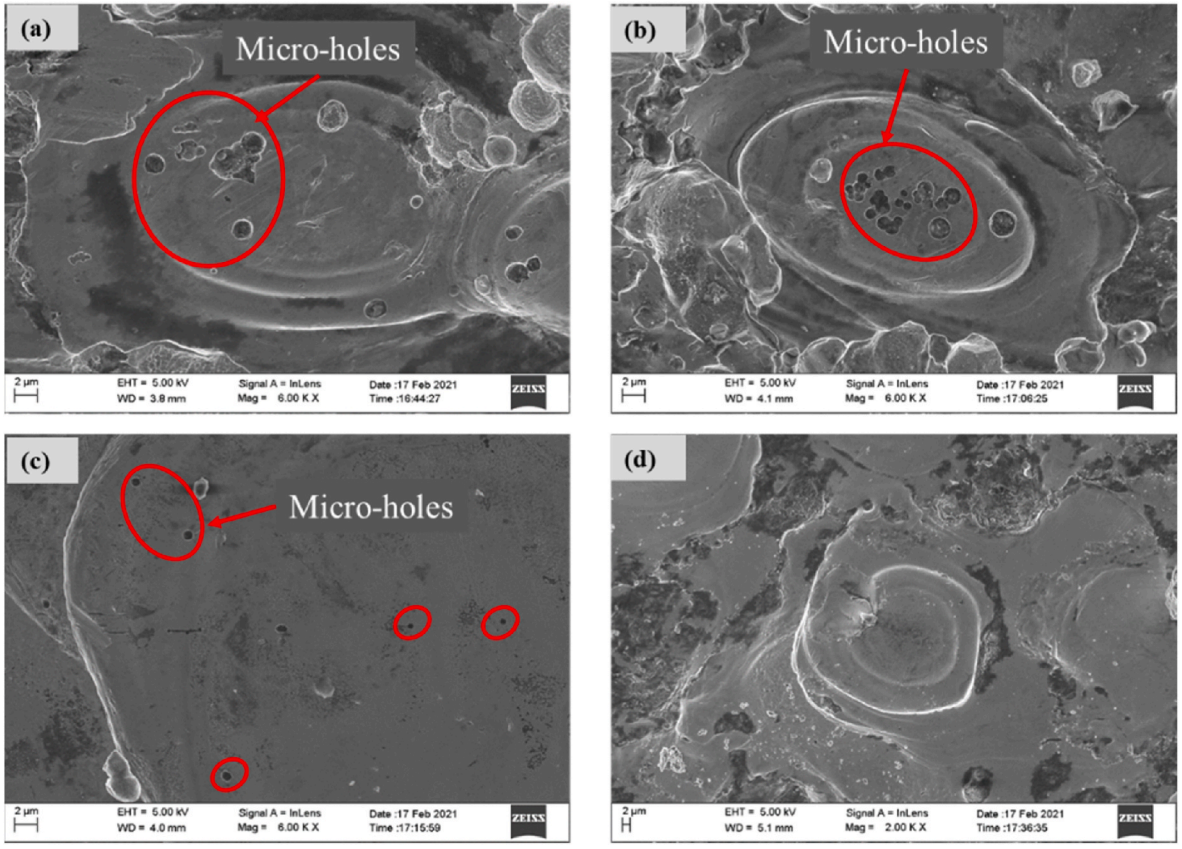

Fig. 13. Microholes over the machined surface at the following conditions: (a) conventional EDM at 8 µs, 2A and 50V, (b) NSMEDM at 8 µs, 2A and 50V, (c) conventional EDM at 8 µs, 6A and 10V, (b) NSMEDM at 8 µs, 6A and 10V

effect on the overall distribution of residual stresses underneath the white layer [75,76]. This phenomenon occurs due to the comparatively small magnitude of these stresses, with the majority of them being evened out in the last stages of the solid-liquid boundary integration subsequent following the discharge operation [70,77,78].

All in all, in the aviation and aircraft sectors, Inconel 718 is widely utilised for numerous uses, notably in the production of jet engines and high-speed aircraft components [79–81]. Such components include fasteners, connectors, screws, nuts, rivet fixings, bolts, buckets, container vessels, instrumentation components, wheels, separators, and spacers [82–84]. Furthermore, it is employed in the manufacture of cryogenic tankage and gasoline turbine blades. In addition, and as indicated by aforementioned findings of the current work, nanofluids have emerged as a superior alternative to conventional fluids. The base dielectric medium influences their performance. These fluids find extensive applications in both traditional and non-traditional machining processes [85,86]. The enhanced thermal conductivity of nanofluids is attributed to the increased specific surface area of the powder particles [87]. Additionally, reducing particle size contributes to achieving a better surface finish. Incorporating conductive nanoparticles further enhances the electrical conductivity of nanofluids, ultimately boosting the performance of EDM [88]. Therefore, analysing the utilisation of nano-sized conductive particles with a high specific surface area is crucial.

4. Conclusions

The experimental investigation focused on the utilisation of graphene nanosheets mixed with a dielectric medium in EDM on Inconel 718 material. Gap voltage, Ton, and Ip were selected as input parameters for the experiment. The response values included MRR, surface roughness (Ra, Tq, and Rz), debris analysis, phase analysis, and residual analysis. The surface morphology of the machined surface was thoroughly examined, revealing the impact of NSMEDM and conventional EDM on the microstructure of the machined surface. The results were obtained at magnifications of 2KX, 6KX, and 10KX to ensure clear visibility of the surface texture and recast layer thickness.

Significant improvements were observed in MRR and surface roughness, with increases of 114.29, 31.47, 35.885, and 37.91 % based on measurement results. In terms of debris analysis, NSMEDM exhibited a maximum debris size range of 10–100 µm, while conventional EDM displayed a range of 100–1000 µm, indicating a reduction of debris size particles by 48.4 % in NSMEDM.

Residual stress analysis revealed that NSMEDM produced a minimum stress of −113.29 MPa, whereas conventional EDM yielded a minimum stress of 110.97 MPa. Maximum residual stresses were measured at 530.61 MPa for NSMEDM and 851.67 MPa for conventional EDM.

The conventional EDM process exhibited the presence of numerous globules on the machined surface under specific conditions (8µs, 2A, 50V and 8µs, 6A, 10V). Conversely, NSMEDM showcased fewer and smaller voids compared to conventional EDM.

Recast layer thickness experienced a reduction of 47.14 and 75.05 % under lower discharge energy conditions (8µs, 2A, 50V) and higher discharge energy conditions (8µs, 6A, 10V), respectively.

Moreover, Vickers hardness of the machined surface increased by 32.64 and 100.4 % in conventional EDM and NSMEDM, respectively.

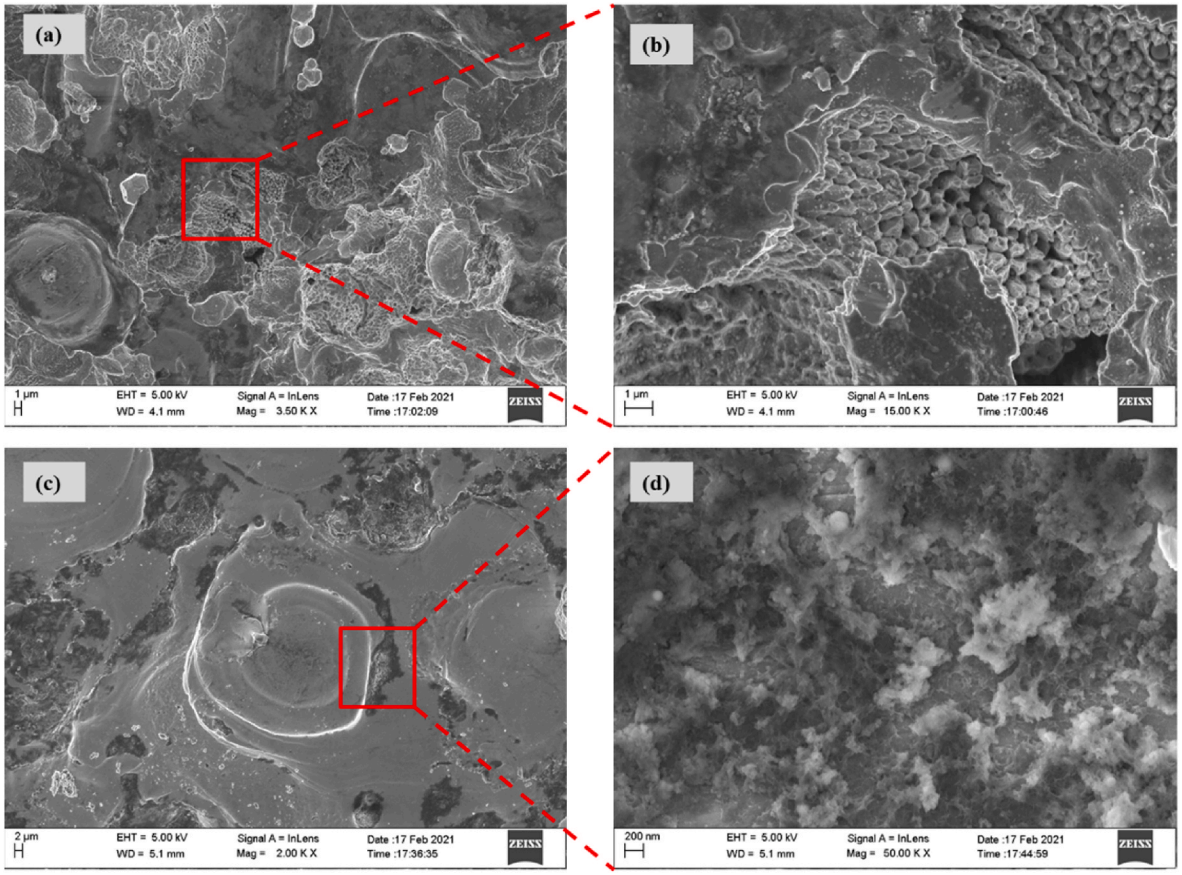

Fig. 14. Surface texture of machined surface at the following conditions: (a) conventional EDM at 8 μs, 2A and 50V, (b) NSMEDM at 8 μs, 2A and 50V, (c) conventional EDM at 8 μs, 6A and 10V, (b) NSMEDM at 8 μs, 6A and 10V.

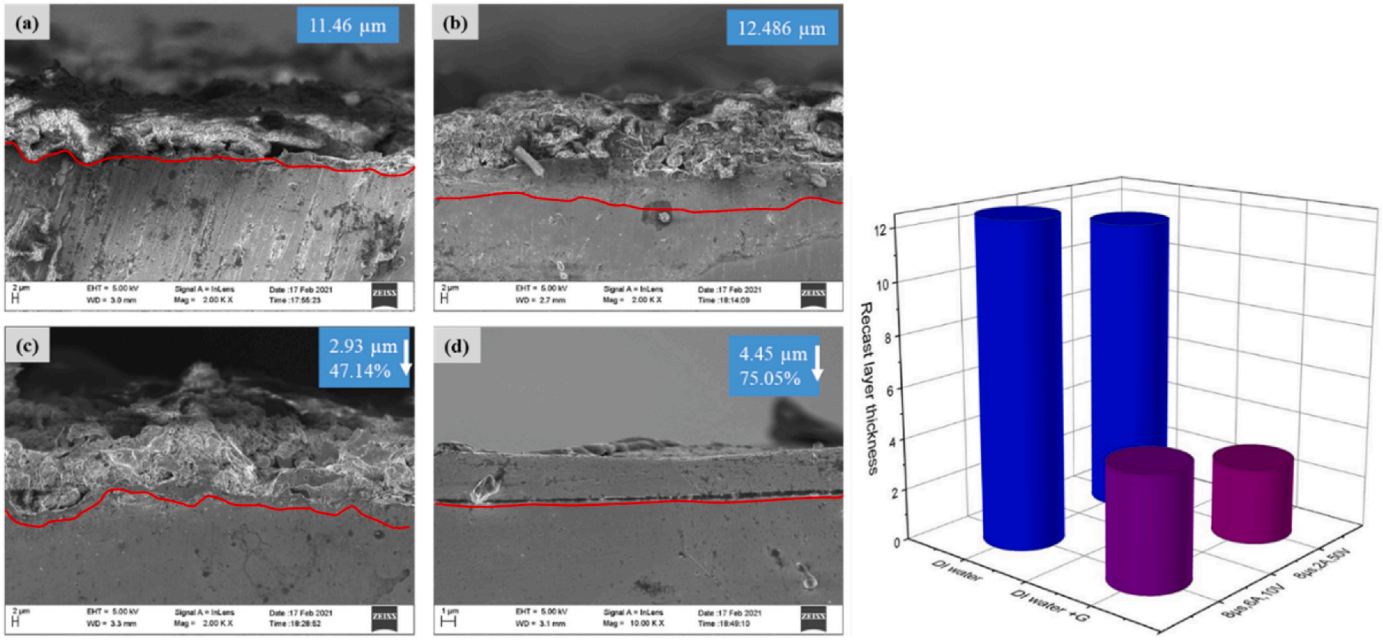

Fig. 15. A cross-section cut of the machined surface of Inconel 718 using (a) conventional EDM at 8 μs, 2A and 50V, (b) NSMEDM at 8 μs, 2A and 50V, (c) conventional EDM at 8 μs, 6A and 10V, (b) NSMEDM at 8 μs, 6A and 10V.

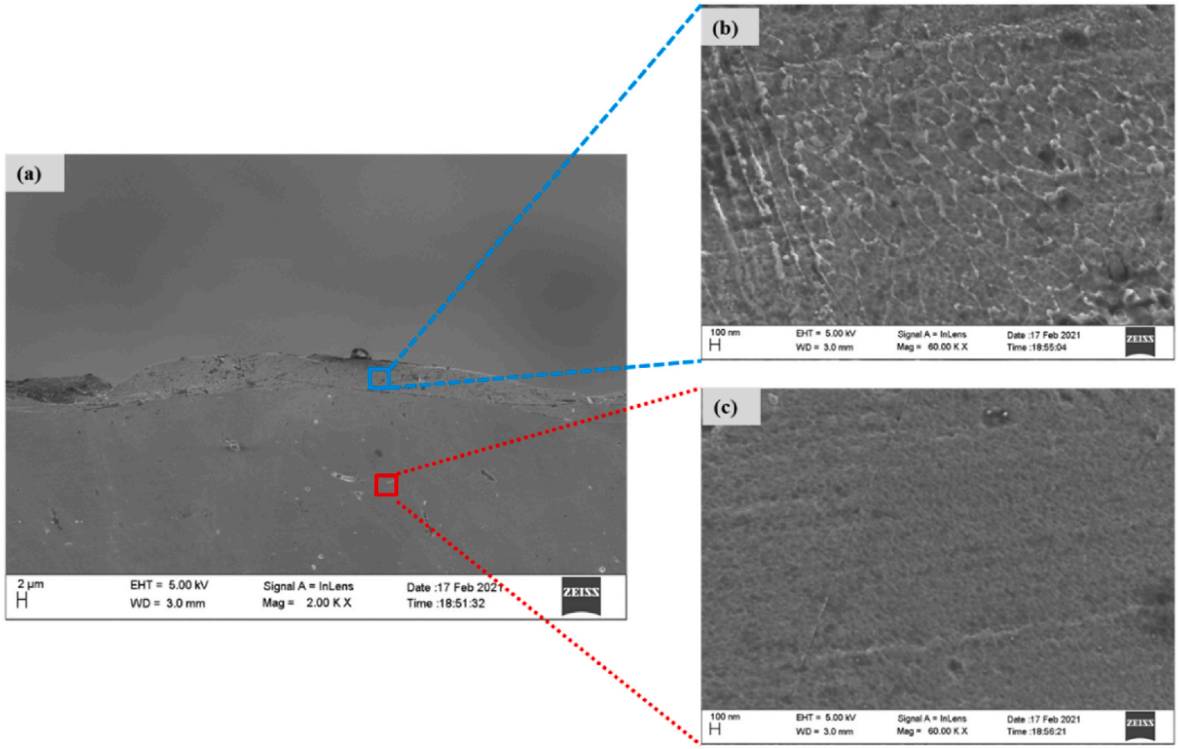

Fig. 16. Microstructure of the recast layer (a) cross-section part of machined surface, (b) microstructure of recast layer and (c) microstructure of base material.

Ethics declarations

Ethical approval

Not applicable.

Consent to participate

Not applicable.

Consent to publish

All authors have read and approved this manuscript.

Data availability statement

The data that support the findings of this study are available within the manuscript.

Funding

The authors extend their appreciation to the Ministry of Education in KSA for funding this research work through the project number KKU-IFP2-DB-6.

Declaration of interests

The authors declare that they have no known competing financial interests or personal relationships that could have appeared to influence the work reported in this paper.

Acknowledgments

The authors extend their appreciation to the Ministry of Education in KSA for funding this research work through the project number KKU-IFP2-DB-6.

References

[1] Ya\csar H, Ekmekci B. Ti-6Al-4V surfaces in SiC powder mixed electrical discharge machining. Mater. Sci. Eng. Technol. II 2014;856:226–30. https://doi.org/10.4028/www.scientific.net/AMR.856.226. Trans Tech Publications Ltd.
[2] Mohammadzadeh Sari M, Noordin MY, Brusa E. Role of multi-wall carbon nanotubes on the main parameters of the electrical discharge machining (EDM) process. Int J Adv Manuf Technol 2013;68:1095–102. https://doi.org/10.1007/s00170-013-4901-5.
[3] Mohammadzadeh Sari M, Noordin MY, Brusa E. Role of multi-wall carbon nanotubes on the main parameters of the electrical discharge machining (EDM) process. Int J Adv Manuf Technol 2013;68:1095–102. https://doi.org/10.1007/s00170-013-4901-5.
[4] Kozak J, Rozenek M, Dabrowski L. Study of electrical discharge machining using powder-suspended working media. Proc Inst Mech Eng Part B J Eng Manuf 2003;217:1597–602. https://doi.org/10.1243/095440503771909971.
[5] Yih-Fong T, Fu-Chen C. Investigation into some surface characteristics of electrical discharge machined SKD-11 using powder-suspension dielectric oil. J Mater Process Technol 2005;170:385–91. https://doi.org/10.1016/j.jmatprotec.2005.06.006.
[6] Chow HM, Yan BH, Huang FY, Hung JC. Study of added powder in kerosene for the micro-slit machining of titanium alloy using electro-discharge machining. J Mater Process Technol 2000;101:95–103. https://doi.org/10.1016/S0924-0136(99)00458-6.
[7] Singh AK, Kumar S, Singh VP. Effect of the addition of conductive powder in dielectric on the surface properties of superalloy Super Co 605 by EDM process. Int J Adv Manuf Technol 2015;77:99–106. https://doi.org/10.1007/s00170-014-6433-z.
[8] Liew PJ, Yan J, Kuriyagawa T. Carbon nanofiber assisted micro electro discharge machining of reaction-bonded silicon carbide. J Mater Process Technol 2013;213:1076–87. https://doi.org/10.1016/j.jmatprotec.2013.02.004.
[9] Kumar A, Maheshwari S, Sharma C, Beri N. Machining efficiency evaluation of cryogenically treated copper electrode in additive mixed EDM. Mater Manuf Process 2012;27:1051–8. https://doi.org/10.1080/10426914.2011.654151.
[10] Molinetti A, Amorim FL, Soares PC, Czelusniak T. Surface modification of AISI H13 tool steel with silicon or manganese powders mixed to the dielectric in electrical discharge machining process. Int J Adv Manuf Technol 2016;83:1057–68. https://doi.org/10.1007/s00170-015-7613-1.
[11] Henriques E, Pecas P. Influence of silicon powder-mixed dielectric on conventional electrical discharge machining. Int J Mach Tool Manufact 2003;43:1465–71. https://doi.org/10.1016/S0890-6955(03)00169-X.
[12] Kansal HK, Singh S, Kumar P, Engineering M. Effect of silicon powder mixed EDM on machining rate of AISI D2 die steel. J Manuf Process 2007;9:13–22. https://doi.org/10.1016/S1526-6125(07)70104-4.

[13] Chow HM, Yang LD, Lin CT, Chen YF. The use of SiC powder in water as dielectric for micro-slit EDM machining. J Mater Process Technol 2008;195:160–70. https://doi.org/10.1016/j.jmatprotec.2007.04.130.
[14] Ekmekci B, Ersöz Y. How suspended particles affect surface morphology in powder mixed electrical discharge machining (PMEDM). Metall Mater Trans B Process Metall Mater Process Sci 2012;43:1138–48. https://doi.org/10.1007/s11663-012-9700-0.
[15] Kumar S, Dhingra AK, Kumar S. Parametric optimization of powder mixed electrical discharge machining for nickel-based superalloy inconel-800 using response surface methodology. Mech Adv Mater Mod Process 2017;3:1–17. https://doi.org/10.1186/s40759-017-0022-4.
[16] Kibria G, Bhattacharyya B. Analysis on geometrical accuracy of microhole during micro-edm of ti-6al-4v using different dielectrics. AIP Conf Proc 2010;1315:155–60. https://doi.org/10.1063/1.3552411.
[17] Kumar S, Batra U. Surface modification of die steel materials by EDM method using tungsten powder-mixed dielectric. J Manuf Process 2012;14:35–40. https://doi.org/10.1016/j.jmapro.2011.09.002.
[18] Furutania K, Saneto A, Takezawa H, Mohri N, Miyake H. Accretion of titanium carbide by electrical discharge machining with powder suspended in working fluid. Precis Eng 2001;25:138–44. https://doi.org/10.1016/S0141-6359(00)00068-4.
[19] Kumar A, Mandal A, Dixit AR, Das AK. Performance evaluation of Al2O3 nano powder mixed dielectric for electric discharge machining of Inconel 825. Mater Manuf Process 2018;33:986–95. https://doi.org/10.1080/10426914.2017.1376081.
[20] Bai X, Zhang Q, Zhang J, Kong D, Yang T. Machining efficiency of powder mixed near dry electrical discharge machining based on different material combinations of tool electrode and workpiece electrode. J Manuf Process 2013;15:474–82. https://doi.org/10.1016/j.jmapro.2013.09.005.
[21] Bai X, Zhang QH, Yang TY, Zhang JH. Research on material removal rate of powder mixed near dry electrical discharge machining. Int J Adv Manuf Technol 2013;68:1757–66. https://doi.org/10.1007/s00170-013-4973-2.
[22] Zhao Y, Kunieda M, Abe K. Comparison on foil EDM characteristics of single crystal SiC between in deionized water and in EDM oil. Int J Adv Manuf Technol 2016;86:2905–12. https://doi.org/10.1007/s00170-016-8412-z.
[23] Kibria G, Sarkar BR, Pradhan BB, Bhattacharyya B. Comparative study of different dielectrics for micro-EDM performance during microhole machining of Ti-6Al-4V alloy. Int J Adv Manuf Technol 2010;48:557–70. https://doi.org/10.1007/s00170-009-2298-y.
[24] Chen S, Lin M, Huang G, Wang C. Research of the recast layer on implant surface modified by micro-current electrical discharge machining using deionized water mixed with titanium powder as dielectric solvent. Appl Surf Sci 2014;311:47–53. https://doi.org/10.1016/j.apsusc.2014.04.204.
[25] Takino H, Ichinohe T, Tanimoto K, Yamaguchi S, Nomura K, Kunieda M. Cutting of polished single-crystal silicon by wire electrical discharge machining. Precis Eng 2004;28:314–9. https://doi.org/10.1016/j.precisioneng.2003.12.002.
[26] Wong Y, Lim L, Rahuman I, Tee W. Near-mirror-finish phenomenon in EDM using powder-mixed dielectric. J Mater Process Technol 1998;79:30–40. https://doi.org/10.1016/S0924-0136(97)00450-0.
[27] Benavides GL, Bieg LF, Saavedra MP, Bryce EA. High aspect ratio meso-scale parts enabled by wire micro-EDM. Microsyst Technol 2002;8:395–401. https://doi.org/10.1007/s00542-002-0190-x.
[28] Jahan MP, Rahman M, Wong YS. Study on the nano-powder-mixed sinking and milling micro-EDM of WC-Co. Int J Adv Manuf Technol 2011;53:167–80. https://doi.org/10.1007/s00170-010-2826-9.
[29] Kolli M, Kumar A. Effect of dielectric fluid with surfactant and graphite powder on Electrical Discharge Machining of titanium alloy using Taguchi method. Eng Sci Technol an Int J 2015;18. https://doi.org/10.1016/j.jestch.2015.03.009. 524–35.
[30] Liew PJ, Yan J, Kuriyagawa T. Fabrication of deep micro-holes in reaction-bonded SiC by ultrasonic cavitation assisted micro-EDM. Int J Mach Tool Manufact 2014;76:13–20. https://doi.org/10.1016/j.ijmachtools.2013.09.010.
[31] Zhao WS, Meng QG, Wang ZL. The application of research on powder mixed EDM in rough machining. J Mater Process Technol 2002;129:30–3.
[32] Bhattacharya A, Batish A, Singh G, Singla VK. Optimal parameter settings for rough and finish machining of die steels in powder-mixed EDM. Int J Adv Manuf Technol 2012;61:537–48. https://doi.org/10.1007/s00170-011-3716-5.
[33] Batish A, Bhattacharya A, Singla VK, Singh G. Study of material transfer mechanism in die steels using powder mixed electric discharge machining. Mater Manuf Process 2012;27:449–56. https://doi.org/10.1080/10426914.2011.585498.
[34] Jeswani ML. Effect of the addition of graphite powder to kerosene used as the dielectric fluid in electrical discharge machining. Wear 1981;70:133–9. https://doi.org/10.1016/0043-1648(81)90148-4.
[35] Prihandana GS, Mahardika M, Hamdi M, Wong YS, Miki N, Mitsui K. Study of workpiece vibration in powder-suspended dielectric fluid in micro-EDM processes. Int J Precis Eng Manuf 2013;14:1817–22. https://doi.org/10.1007/s12541-013-0243-3.
[36] Wu KL, Yan BH, Huang FY, Chen SC. Improvement of surface finish on SKD steel using electro-discharge machining with aluminum and surfactant added dielectric. Int J Mach Tool Manufact 2005;45:1195–201. https://doi.org/10.1016/j.ijmachtools.2004.12.005.
[37] Tzeng YF, Lee CY. Effects of powder characteristics on electrodischarge machining efficiency. Int J Adv Manuf Technol 2001;17:586–92. https://doi.org/10.1007/s001700170142.
[38] Kansal HK, Singh S, Kumar P. Parametric optimization of powder mixed electrical discharge machining by response surface methodology. J Mater Process Technol 2005;169:427–36. https://doi.org/10.1016/j.jmatprotec.2005.03.028.
[39] Peças P, Henriques E. Effect of the powder concentration and dielectric flow in the surface morphology in electrical discharge machining with powder-mixed dielectric (PMD-EDM). Int J Adv Manuf Technol 2008;37:1120–32. https://doi.org/10.1007/s00170-007-1061-5.
[40] Chen YF, Lin YC. Surface modifications of Al-Zn-Mg alloy using combined EDM with ultrasonic machining and addition of TiC particles into the dielectric. J Mater Process Technol 2009;209:4343–50. https://doi.org/10.1016/j.jmatprotec.2008.11.013.
[41] Prihandana GS, Mahardika M, Hamdi M, Wong YS, Mitsui K. Effect of micro-powder suspension and ultrasonic vibration of dielectric fluid in micro-EDM processes-Taguchi approach. Int J Mach Tool Manufact 2009;49:1035–41. https://doi.org/10.1016/j.ijmachtools.2009.06.014.
[42] Garg RK, Ojha K. Parametric optimization of PMEDM process with chromium powder suspended dielectric for triangular electrodes. Adv Mater Res 2013;816–817:23–7. https://doi.org/10.4028/www.scientific.net/AMR.816-817.23.
[43] Hu FQ, Cao FY, Song BY, Hou PJ, Zhang Y, Chen K, et al. Surface properties of SiCp/Al composite by powder-mixed EDM. Procedia CIRP 2013;6:101–6. https://doi.org/10.1016/j.procir.2013.03.036.
[44] Klocke F, Lung D, Antonoglou G, Thomaidis D. The effects of powder suspended dielectrics on the thermal influenced zone by electrodischarge machining with small discharge energies. J Mater Process Technol 2004;149:191–7. https://doi.org/10.1016/j.jmatprotec.2003.10.036.
[45] Bhattacharya A, Batish A, Kumar N. Surface characterization and material migration during surface modification of die steels with silicon, graphite and tungsten powder in EDM process. J Mech Sci Technol 2013;27:133–40. https://doi.org/10.1007/s12206-012-0883-8.
[46] Baseri H, Sadeghian S. Effects of nanopowder TiO2-mixed dielectric and rotary tool on EDM. Int J Adv Manuf Technol 2016;83:519–28. https://doi.org/10.1007/s00170-015-7579-z.
[47] Moudood MA, Sabur A, Mohammad YA, Jaafar IH. Effect of peak current on material removal rate for electrical discharge machining of non-conductive Al2O3 ceramic. Adv Mater Res 2014;845:730–4. https://doi.org/10.4028/www.scientific.net/AMR.845.730.
[48] Garg SK, Manna A, Jain A. Experimental investigation of spark gap and material removal rate of Al/ZrO2(P)-MMC machined with wire EDM. J Brazilian Soc Mech Sci Eng 2016;38:481–91. https://doi.org/10.1007/s40430-015-0394-5.
[49] Sanchez JA, Plaza S, Lacalle LNL De, Lamikiz A. Computer simulation of wire-EDM taper-cutting. Int J Comput Integrated Manuf 2006;19:727–35. https://doi.org/10.1080/09511920600628855.
[50] Sanchez JA, de Lacalle LNL, Lamikiz A. A computer-aided system for the optimization of the accuracy of the wire electro-discharge machining process. Int J Comput Integrated Manuf 2004;17:413–20. https://doi.org/10.1080/09511920310001626590.
[51] Chaudhari R, Vora JJ, Patel V, de Lacalle LNL, Parikh DM. Effect of wedm process parameters on surface morphology of nitinol shape memory alloy. Materials 2020;13:1–14. https://doi.org/10.3390/ma13214943.
[52] Prabhu S, Vinayagam BK. AFM nano analysis of inconel 825 with single wall carbon nano tube in die sinking EDM process using taguchi analysis. Arabian J Sci Eng 2013;38:1599–613. https://doi.org/10.1007/s13369-012-0348-5.
[53] Mai C, Hocheng H, Huang S. Advantages of carbon nanotubes in electrical discharge machining. Int J Adv Manuf Technol 2012;59:111–7. https://doi.org/10.1007/s00170-011-3476-2.
[54] Marashi H, Sarhan AAD, Hamdi M. Employing Ti nano-powder dielectric to enhance surface characteristics in electrical discharge machining of AISI D2 steel. Appl Surf Sci 2015;357:892–907. https://doi.org/10.1016/j.apsusc.2015.09.105.
[55] Jin JC, Cho S, Kim K, Sim H, Park BG, Lee YK. Microstructures and intergranular corrosion resistances of hot-rolled austenitic stainless steel clad plates. J Mater Res Technol 2023;26:1–13. https://doi.org/10.1016/j.jmrt.2023.07.192.
[56] Mohal S, Kumar H. Parametric optimization of multiwalled carbon nanotube-assisted electric discharge machining of Al-10%SiCp metal matrix composite by response surface methodology. Mater Manuf Process 2017;32:263–73. https://doi.org/10.1080/10426914.2016.1140196.
[57] Shabgard M, Khosrozadeh B. Investigation of carbon nanotube added dielectric on the surface characteristics and machining performance of Ti–6Al–4V alloy in EDM process. J Manuf Process 2017;25:212–9. https://doi.org/10.1016/j.jmapro.2016.11.016.
[58] Talla G, Gangopadhyay S, Biswas CK. Effect of powder-suspended dielectric on the EDM characteristics of inconel 625. J Mater Eng Perform 2016;25:704–17. https://doi.org/10.1007/s11665-015-1835-0.
[59] Chen SL, Hsieh SF, Lin HC, Lin MH, Huang JS. Electrical discharge machining of a NiAlFe ternary shape memory alloy. J Alloys Compd 2008;464:446–51. https://doi.org/10.1016/j.jallcom.2007.10.012.
[60] Lin HC, Lin KM, Chen YC. The electro-discharge machining characteristics of TiNi shape memory alloys. J Mater Process Technol 2000;105:327–32. https://doi.org/10.1016/S0924-0136(00)00656-7.
[61] Arnell RD, Merdan MAE-R, Arnell RD. The surface integrity of a die steel after electrodischarge machining: 2 residual stress distribution. Surf Eng 1991;7:154–8. https://doi.org/10.1179/sur.1991.7.2.154.
[62] Gill AS, Kumar S. Surface roughness and microhardness evaluation for EDM with Cu-Mn powder metallurgy tool. Mater Manuf Process 2016;31:514–21. https://doi.org/10.1080/10426914.2015.1070412.
[63] Kumar S, Singh R. Investigating surface properties of OHNS die steel after electrical discharge machining with manganese powder mixed in the dielectric.

Int J Adv Manuf Technol 2010;50:625–33. https://doi.org/10.1007/s00170-010-2536-3.
[64] Sharma P, Chakradhar D, Narendranath S. Evaluation of WEDM performance characteristics of Inconel 706 for turbine disk application. Mater Des 2015;88:558–66. https://doi.org/10.1016/j.matdes.2015.09.036.
[65] Hosseini Monazzah A, Pouraliakbar H, Bagheri R, Seyed Reihani SM. Al-Mg-Si/SiC laminated composites: fabrication, architectural characteristics, toughness, damage tolerance, fracture mechanisms. Composites Part B 2017;125:49–70. https://doi.org/10.1016/j.compositesb.2017.05.055.
[66] Chaudhari Rakesh, Vora Jay J, Patel Vivek, López de Lacalle LN, Parikh DM. Surface analysis of wire-electrical-discharge-machining-processed shape-memory alloys. Materials 2020;13(3):530. https://doi.org/10.3390/ma13030530.
[67] Muthuramalingam T. Measuring the influence of discharge energy on white layer thickness in electrical discharge machining process. Measurement 2019;131:694–700.
[68] Klocke Fritz, Hensgen Lars, Klink Andreas, Ehle Lisa, Alexander Schwedt. Structure and composition of the white layer in the wire-EDM process. Procedia CIRP 2016;42:673–8.
[69] Sahu Santosh Kumar, Datta Saurav. Experimental studies on graphite powder-mixed electro-discharge machining of Inconel 718 super alloys: comparison with conventional electro-discharge machining. Proc IME E J Process Mech Eng 2019;233(2):384–402.
[70] Ekmekci Bülent. Residual stresses and white layer in electric discharge machining (EDM). Appl Surf Sci 2007;253(23):9234–40.
[71] Paswan K, Pramanik A, Chattopadhyaya S, Sharma S, Singh G, Khan AM, et al. An analysis of machining response parameters, crystalline structures, and surface topography during EDM of die-steel using EDM oil and liquid-based viscous dielectrics: a comparative analysis of machining performance. Arabian J Sci Eng 2023. https://doi.org/10.1007/s13369-023-07626-x.
[72] Amoljit Singh Gill, Kumar Sanjeev, Singh Jujhar, Agarwal Vivek, Sharma S. A review of recent methods for tool wear reduction in electrical discharge machining. Surface Review and Letters (SRL)-World Scientific Publishers 2020. https://doi.org/10.1142/S0218625X20300026.
[73] Zhang X, Li C, Zhou Z, Liu B, Zhang Y B, Min Y, et al. H.Vegetable Oil-Based Nanolubricants in Machining: From Physicochemical Properties to Application. Chin J Mech Eng 2023;36:76. https://doi.org/10.1186/s10033-023-00895-5.
[74] Singh Gurpreet, Sehijpal Singh, Sharma S, Singh Jujhar, Li Chang, Krolczyk Grzegorz, et al. Performance investigations for sustainability assessment of Hastelloy C-276 under different machining environments. Heliyon 2023;9:e13933. https://doi.org/10.1016/j.heliyon.2023.e13933.
[75] Wenhao Xu, C Li, Yanbin Zhang, Hafiz Muhammad Ali, S Sharma, Runze Li, Min Yang, Teng Gao, Mingzheng Liu, Xiaoming Wang, Zafar Said, Xin Liu, Zongming Zhou. Electrostatic atomization minimum quantity lubrication machining: from mechanism to application. Int J Extrem Manuf. https://doi.org/10.1088/2631-7990/ac9652.
[76] Saravanan R, Sathish T, Vijayan V, Rajkumar S, Sharma S, Li C, et al. Eco-friendly MoS2/waste coconut oil nanofluid for machining of magnesium implants. Rev Adv Mater Sci 2023;62(1):20220296. https://doi.org/10.1515/rams-2022-0296.
[77] Raj Atul, Misra JP, Singh Ravinder Pal, Singh Gurminder, Sharma S, Eldin SM. Performance analysis of WEDM during the machining of Inconel 690 miniature gear using RSM and ANN modeling approaches. Reviews on Advanced Materials Science. De Gruyter); 2022. https://doi.org/10.1515/rams-2022-0288.
[78] Wang, Xiaoming & Song, Yuxiang & Li, Chang & Zhang, Y B & Ali, Hafiz & Sharma, S & Li, Runze & Min, Yang & Gao, Teng & Liu, Mingzheng & Cui, Xin & Said, Zafar & Zhou, Zongming. (2023). Nanofluids application in machining: a comprehensive review. The International J Adv Man Tech. 10.1007/s00170-022-10767-2.
[79] Singh Gurpreet, Aggarwal Vivek, Singh Sehijpal, Singh Balkar, Sharma S, Singh Jujhar, et al. Experimental investigation and performance optimization during machining of Hastelloy C-276 using green lubricants. Materials (MDPI). Materials 2022;15(15):5451. https://doi.org/10.3390/ma15155451. 2022.
[80] Mingzheng LIU, Li C, Yanbin ZHANG, Qinglong AN, Min YANG, Teng GAO, et al. Cryogenic minimum quantity lubrication machining: from mechanism to application. Front Mech Eng 2021;16(4):649–97. https://doi.org/10.1007/s11465-021-0654-2.
[81] Cui Xin, Li C, Ding Wenfeng, Chen Yun, Mao Cong, Xu Xuefeng, et al. Minimum quantity lubrication machining of aeronautical materials using carbon group nanolubricant: from mechanisms to application. Chin J Aeronaut 2021. https://doi.org/10.1016/j.cja.2021.08.011.
[82] Mashood Khan Aqib, Alkahtani Mohammed, Sharma S, Jamil Muhammad, Iqbal Asif, Ning He. Sustainability-based holistic assessment and determination of optimal resource consumption for energy-efficient machining of hardened steel. J Clean Prod 2021. https://doi.org/10.1016/j.jclepro.2021.128674.
[83] Pramanik A, Basak AK, Prakash C, Shankar S, Sharma S, Narendranath S. Recast layer formation during wire electrical discharge machining (WEDM) of titanium (Ti-Al6-V4) alloy. J Mater Eng Perform 2021. https://doi.org/10.1007/s11665-021-06116-1.
[84] Kumar J, Sharma S, Singh J, Singh S, Singh G. Optimization of wire-EDM process parameters for Al-Mg-0.6Si-0.35Fe/15%RHA/5%Cu hybrid metal matrix composite using TOPSIS: processing and characterizations. J. Manuf. Mater. Process. 2022;6:150. https://doi.org/10.3390/jmmp6060150.
[85] Muni Ram Narayan, Singh Jujhar, Kumar Vineet, Sharma S, Sudhakara P, Aggarwal Vivek, et al. Multi-objective optimization of EDM parameters for Rice husk Ash/Cu/Mg reinforced hybrid Al- 0.7Fe-0.6Si-0.375Cr-0.25Zn metal-matrix nanocomposites for Engineering applications: fabrication, and Morphological Analysis. J Nanomater 2022. https://doi.org/10.1155/2022/2188705.
[86] V Aggarwal, C I Pruncu, J Singh, S Sharma, DY Pimenov. Empirical investigations during WEDM of Ni-27Cu-3.15Al-2Fe-1.5Mn based superalloy using Response Surface Methodology for high temperature corrosion resistance applications. Materials (MDPI) Journal, 13, 3470 (1–18); DOI: https://10.3390/ma13163470.
[87] Garg HK, Sharma S, Kumar R, Manna A, C Li K Mausam, Eldin EMT. "Multi-objective parametric optimization on the EDM machining of hybrid SiCp/Grp/Aluminum nanocomposites using Non-dominating Sorting Genetic Algorithm (NSGA-II). Fabrication and Microstructural Characterizations" Reviews on Advanced Materials Science (De Gruyter) 2022;61:1–24. https://doi.org/10.1515/rams-2022-0279.
[88] S Sharma, P Sudhakara "Fabrication and optimization of hybrid AA-6082-T6 alloy/8%Al2O3(Alumina)/2%Grp metal matrix composites using novel Box-Behnken methodology processed by wire- sinking electric discharge machining" Materials Research Express. https://doi.org/10.1088/2053-1591/ab4b97.
[89] Wu Y, Chen J, Zhang L, Ji J, Wang Q, Zhang S. Effect of boron on the structural stability, mechanical properties, and electronic structures of γ′-Ni3Al in TLP joints of nickel-based single-crystal alloys. Mater Today Commun 2022;31:103375. https://doi.org/10.1016/j.mtcomm.2022.103375.
[90] Zhao W, Suo H, Wang S, Ma L, Wang L, Wang Q, et al. Mg gas infiltration for the fabrication of MgB2 pellets using nanosized and microsized B powders. J Eur Ceram Soc 2022. https://doi.org/10.1016/j.jeurceramsoc.2022.08.029.
[91] Wang D, Wang X, Jin ML, He P, Zhang S. Molecular level manipulation of charge density for solid-liquid TENG system by proton irradiation. Nano Energy 2022;103:107819. https://doi.org/10.1016/j.nanoen.2022.107819.
[92] Liao D, Zhu S, Keshtegar B, Qian G, Wang Q. Probabilistic framework for fatigue life assessment of notched components under size effects. Int J Mech Sci 2020;181:105685. https://doi.org/10.1016/j.ijmecsci.2020.105685.
[93] Niu X, Zhu S, He J, Liao D, Correia JAFO, Berto F, et al. Defect tolerant fatigue assessment of AM materials: size effect and probabilistic prospects. Int J Fatig 2022;160:106884. https://doi.org/10.1016/j.ijfatigue.2022.106884.
[94] Niu X, Zhu S, He J, Liao D, Correia JAFO, Berto F, et al. Defect tolerant fatigue assessment of AM materials: size effect and probabilistic prospects. Int J Fatig 2022;160:106884. https://doi.org/10.1016/j.ijfatigue.2022.106884.
[95] Yuhua C, Yuqing M, Weiwei L, Peng H. Investigation of welding crack in micro laser welded NiTiNb shape memory alloy and Ti6Al4V alloy dissimilar metals joints. Opt Laser Technol 2017;91:197–202. https://doi.org/10.1016/j.optlastec.2016.12.028.
[96] Zhang Z, Chen J, Wang J, Han Y, Yu Z, Wang Q, et al. Effects of solder thickness on interface behavior and nanoindentation characteristics in Cu/Sn/Cu microbumps. Weld World 2022;66(5):973–83. https://doi.org/10.1007/s40194-022-01261-0.
[97] Guo K, Gou G, Lv H, Shan M. Jointing of CFRP/5083 aluminum alloy by induction brazing: processing, connecting mechanism, and fatigue performance. Coatings 2022;12(10):1559. https://doi.org/10.3390/coatings12101559.
[98] Fu ZH, Yang BJ, Shan ML, Li T, Zhu ZY, Ma CP, et al. Hydrogen embrittlement behavior of SUS301L-MT stainless steel laser-arc hybrid welded joint localized zones. Corrosion Sci 2020;164:108337. https://doi.org/10.1016/j.corsci.2019.108337.
[99] Zhu ZY, Liu YL, Gou GQ, Gao W, Chen J. Effect of heat input on interfacial characterization of the butter joint of hot-rolling CP-Ti/Q235 bimetallic sheets by Laser + CMT. Sci Rep 2021;11(1):10020. https://doi.org/10.1038/s41598-021-89343-9.
[100] Zhu Q, Chen J, Gou G, Chen H, Li P. Ameliorated longitudinal critically refracted—attenuation velocity method for welding residual stress measurement. J Mater Process Technol 2017;246:267–75. https://doi.org/10.1016/j.jmatprotec.2017.03.022.
[101] Chen Y, Sun S, Zhang T, Zhou X, Li S. Effects of post-weld heat treatment on the microstructure and mechanical properties of laser-welded NiTi/304SS joint with Ni filler. Mater Sci Eng, A 2020;771:138545. https://doi.org/10.1016/j.msea.2019.138545.
[102] Yang K, Yu H, Cao X, Guan J, Cai S, Yang Z, et al. The critical role of corrugated lamellae morphology on the tough mechanical performance of natural Syncerus caffer horn sheath. Cell Reports Physical Science 2023:101576. https://doi.org/10.1016/j.xcrp.2023.101576.
[103] Zhao P, Zhu J, Yang K, Li M, Shao G, Lu H, et al. Outstanding wear resistance of plasma sprayed high-entropy monoboride composite coating by inducing phase structural cooperative mechanism. Appl Surf Sci 2023;616:156516. https://doi.org/10.1016/j.apsusc.2023.156516.
[104] Ma G, He P, Wang H, Tian H, Zhou L, Yong Q, et al. Promoting bonding strength between internal Al-Si based gradient coating and aluminum alloy cylinder bore by forming homo-epitaxial growth interface. Mater Des 2023;227:111764. https://doi.org/10.1016/j.matdes.2023.111764.
[105] He HT, Fang JX, Wang JX, Sun T, Yang Z, Ma B, et al. Carbide-reinforced Re0.1Hf0.25NbTaW0.4 refractory high-entropy alloy with excellent room and elevated temperature mechanical properties. Int J Refract Metals Hard Mater 2023:106349. https://doi.org/10.1016/j.ijrmhm.2023.106349.
[106] Dong Y, Shao P, Guo X, Xu B, Yin C, Tan Z. Deformation characterization method of typical double-walled turbine blade structure during casting process. J Iron Steel Res Int 2023. https://doi.org/10.1007/s42243-022-00897-y.
[107] Yang K, Qin N, Yu H, Zhou C, Deng H, Tian W, et al. Correlating multi-scale structure characteristics to mechanical behavior of Caprinae horn sheaths. J Mater Res Technol 2022;21:2191–202. https://doi.org/10.1016/j.jmrt.2022.10.044.
[108] Zhao J, Zhou M, Chen J, Wang L, Zhang Q, Zhong S, et al. Two birds one stone: graphene assisted reaction kinetics and ionic conductivity in phthalocyanine-

based covalent organic framework anodes for lithium-ion batteries. Small 2023: 2303353. https://doi.org/10.1002/smll.202303353.
[109] Zhang L, Li J, Xiong D, Xu M, Yin L, Zhang H, et al. Dynamic growth mechanism of tin whisker driven by compressive stress under thermal-mechanic-electric-diffusion coupling. Vacuum 2023;215:112299. https://doi.org/10.1016/j.vacuum.2023.112299.
[110] Zhang H, Xiao Y, Xu Z, Yang M, Zhang L, Yin L, et al. Effects of Ni-decorated reduced graphene oxide nanosheets on the microstructural evolution and mechanical properties of Sn-3.0Ag-0.5Cu composite solders. Intermetallics 2022; 150:107683. https://doi.org/10.1016/j.intermet.2022.107683.
[111] Hua Y, Li F, Hu N, Fu S. Frictional characteristics of graphene oxide-modified continuous glass fiber reinforced epoxy composite. Compos Sci Technol 2022; 223:109446. https://doi.org/10.1016/j.compscitech.2022.109446.
[112] Guo H, Zhang J. Expansion of sandwich tubes with metal foam core under axial compression. J Appl Mech 2023;90(5). https://doi.org/10.1115/1.4056686.
[113] Liu M, Huang J, Meng H, Liu C, Chen Z, Yang H, et al. A novel approach to prepare graphite nanoplatelets exfoliated by three-roll milling in phenolic resin for low-carbon MgO-C refractories. J Eur Ceram Soc 2023;43(9):4198–208. https://doi.org/10.1016/j.jeurceramsoc.2023.02.064.
[114] Hu J, Yang K, Wang Q, Chen Zhao Q, Hui Jiang Y, Jie Liu Y. Ultra-long life fatigue behavior of a high-entropy alloy. Int J Fatig 2023. https://doi.org/10.1016/j.ijfatigue.2023.108013.
[115] Xie B, Li H, Ning Y, Fu M. Discontinuous dynamic recrystallization and nucleation mechanisms associated with 2-, 3- and 4-grain junctions of polycrystalline nickel-based superalloys. Mater Des 2023;231:112041. https://doi.org/10.1016/j.matdes.2023.112041.
[116] Gao S, Li H, Huang H, Kang R. Grinding and lapping induced surface integrity of silicon wafers and its effect on chemical mechanical polishing. Appl Surf Sci 2022; 599:153982. https://doi.org/10.1016/j.apsusc.2022.153982.
[117] Chen L, Zhao Y, Li M, Li L, Hou L, Hou H. Reinforced AZ91D magnesium alloy with thixomolding process facilitated dispersion of graphene nanoplatelets and enhanced interfacial interactions. Mater Sci Eng, A 2021;804:140793. https://doi.org/10.1016/j.msea.2021.140793.
[118] Li M, Guo Q, Chen L, Li L, Hou H, Zhao Y. Microstructure and properties of graphene nanoplatelets reinforced AZ91D matrix composites prepared by electromagnetic stirring casting. J Mater Res Technol 2022;21:4138–50. https://doi.org/10.1016/j.jmrt.2022.11.033.
[119] Zhao Y. Understanding and design of metallic alloys guided by phase-field simulations. npj Comput Mater 2023;9(1):94. https://doi.org/10.1038/s41524-023-01038-z.
[120] Chen L, Zhao Y, Jing J, Hou H. Microstructural evolution in graphene nanoplatelets reinforced magnesium matrix composites fabricated through thixomolding process. J Alloys Compd 2023;940:168824. https://doi.org/10.1016/j.jallcom.2023.168824.
[121] Liu W, Zhao Y, Zhang Y, Shuai C, Chen L, Huang Z, et al. Deformation-induced dynamic precipitation of 14H-LPSO structure and its effect on dynamic recrystallization in hot-extruded Mg-Y-Zn alloys. Int J Plast 2023;164:103573. https://doi.org/10.1016/j.ijplas.2023.103573.
[122] Lashin MMA, Ibrahim MZ, Khan MI, Guedri K, Saxena KK, Eldin SM. Fuzzy control modeling to optimize the hardness and geometry of laser cladded Fe-based MG single track on stainless steel substrate prepared at different surface roughness. Micromachines 2022;13(12):2191. https://doi.org/10.3390/mi13122191.
[123] Dikshit MK, Singh S, Pathak VK, Saxena KK, Agrawal MK, Malik V, et al. Surface characteristics optimization of biocompatible Ti6Al4V with RCCD and NSGA II using die sinking EDM. J Mater Res Technol 2023;24:223–35. https://doi.org/10.1016/j.jmrt.2023.03.005.
[124] Sehar Bakhtawar, Waris Muhammad, Gilani Syed, Ansari Umar, Mushtaq Shafaq, Khan Niaz, et al. The impact of laminations on the mechanical strength of carbon-fiber composites for prosthetic foot fabrication. Crystals 2022;12:1429. https://doi.org/10.3390/cryst12101429.
[125] Singh Bharat, Kumar Indradeep, Saxena Kuldeep, Mohammed Kahtan, Khan M, Ben Moussa Sana, et al. A future prospects and current scenario of aluminium metal matrix composites characteristics. Alex Eng J 2023;76:1–17. https://doi.org/10.1016/j.aej.2023.06.028.
[126] Kumar M, Sathisha N, Manjnatha S, Niranjana, Tamam Nissren. Fatigue surface analysis of AL A356 alloy reinforced hematite metal matrix composites. Biomass Conversion and Biorefinery 2023:1–13. https://doi.org/10.1007/s13399-023-04634-7.
[127] Shahid Muhammad, Javed Hafiz, Muhammad Asif, Ahmad Muhammad, Qureshi Akbar, Khan Muhammad, et al. A brief assessment on recent developments in efficient electrocatalytic nitrogen reduction with 2D non-metallic nanomaterials. Nanomaterials 2022;12. https://doi.org/10.3390/nano12193413. Basel, Switzerland.
[128] Kiranakumar V, Ramakrishnaiah Thejas, Naveen S, Khan M, Gunderi Prasanna, Reddy Sathish, et al. A review on electrical and gas-sensing properties of reduced graphene oxide-metal oxide nanocomposites. Biomass Conversion and Biorefinery 2022. https://doi.org/10.1007/s13399-022-03258-7.
[129] Kumar Rajan, Dwivedi Ravi, Arya Ranjeet, Sonia Pankaj, Yadav Anil, Saxena Kuldeep, et al. Current development of carbide free bainitic and retained austenite on wear resistance in high silicon steel. J Mater Res Technol 2023;24. 10.1016/j.jmrt.2023.05.067.
[130] Prasanthi Phani, Kumar M, Mallampati Somaiah, Madhav V, Saxena Kuldeep, Mohammed Kahtan, et al. Mechanical properties of carbon fiber reinforced with carbon nanotubes and graphene filled epoxy composites: experimental and numerical investigations. Mater Res Express 2023. https://doi.org/10.1088/2053-1591/acaef5. 10.
[131] Vemanaboina H, Babu MM, Prerana IC, Gundabattini E, Yelamasetti B, Saxena KK, et al. Evaluation of residual stresses in CO2 laser beam welding of SS316L weldments using FEA. Mater Res Express 2023;10(1):016509. https://doi.org/10.1088/2053-1591/acb0b5.